MOLECULAR BIOLOGY

A potent and selective ENL degrader suppresses oncogenic gene expression and leukemia progression

Zhaoyu Xue[1]†, Lihuai Qin[2]†, Hongwen Xuan[1]†, Kaixiu Luo[2]†, Mengying Huang[1], Ling Xie[3], Yangzhou Su[1], Longxia Xu[1], Josiah Harsh[1], Brandon Dale[2], Xiaobing Shi[1], Xian Chen[3], H Ümit Kaniskan[2], Jian Jin[2]*, Hong Wen[1]*

The histone acylation reader eleven-nineteen leukemia (ENL) plays a pivotal role in sustaining oncogenesis in acute leukemias, particularly in *mixed-lineage leukemia*–rearranged (*MLL*-r) leukemia. ENL relies on its reader domain to recognize histone lysine acylation promoting oncogenic gene expression and leukemia progression. Here, we report the development of MS41, a highly potent and selective von Hippel–Lindau–recruiting ENL degrader that effectively inhibits the growth of ENL-dependent leukemia cells. MS41-induced ENL degradation reduces the chromatin occupancy of ENL-associated transcription elongation machinery, resulting in the suppression of key oncogenic gene expression programs and the activation of differentiation genes. MS41 is well-tolerated in vivo and substantially suppresses leukemia progression in a xenograft mouse model of *MLL-r* leukemia. Notably, MS41 also induces the degradation of mutant ENL proteins identified in Wilms' tumors. Our findings emphasize the therapeutic potential of pharmacological ENL degradation for treating ENL-dependent cancers, making MS41 not only a valuable chemical probe but also potential anticancer therapeutic for further development.

INTRODUCTION

Despite remarkable progress in leukemia treatments, certain subtypes of acute leukemia, such as the *mixed-lineage leukemia* (*MLL*) gene rearranged (*MLL*-r) leukemia, are refractory to existing therapies, resulting in poor patient outcomes (*1*, *2*). *MLL* (also known as *MLL1*, *ALL-1*, or *KMT2A*) gene disruptions due to chromosomal rearrangements are particularly common in high-risk acute leukemias, notably in infants (*3*). These rearrangements are associated with a dismal prognosis, with up to 80% of infant acute lymphoblastic leukemia (ALL) and 35 to 50% of infant acute myeloid leukemia (AML) cases characterized by *MLL* rearrangements (*4*–*6*). This patient population shows poor responses to standard treatments, underscoring the urgent need for effective therapies.

This study focuses on eleven-nineteen leukemia (ENL, also known as MLLT1 or YEATS1), a histone acylation reader and an essential dependency in acute leukemias (*7*, *8*). ENL and its paralog *ALL1*-fused gene from chromosome 9 (AF9) function as transcriptional coactivators primarily associated with the super elongation complex (SEC) (*9*–*15*) and the complex associated with the histone H3K79 methyltransferase Disruptor of telomeric silencing 1–like (DOT1L) (*15*–*18*), playing key roles in transcription elongation. Both ENL and AF9 contain an evolutionally conserved Yaf9, ENL, AF9, Taf14, and Sas5 (YEATS) domain, which serves as a reader module for histone lysine acylation (*8*, *19*–*22*). Previous studies, including ours, have highlighted the critical role of the full-length wild-type ENL, but not wild-type AF9, in sustaining oncogenic gene expression programs in acute leukemias (*7*, *8*), particularly *MLL*-r leukemia, where MLL fusions "hijack" SEC and the DOT1L complex to drive aberrant leukemogenic gene expression (*23*–*26*). ENL interacts with histone lysine acylation via its YEATS domain, facilitating the recruitment and stabilization of the associated transcriptional machinery for target gene transcription. Genetic depletion of ENL or disruption of the YEATS domain's reader function has shown promise in suppressing leukemia progression, suggesting that ENL is a promising therapeutic target for certain subtypes of acute leukemia (*7*, *8*).

These findings have spurred extensive research efforts aimed at developing potential therapeutics targeting ENL, with our laboratories actively participating in these efforts. The acyl lysine–binding pocket within the ENL YEATS domain presents a druggable pocket for the development of small-molecule inhibitors due to its distinctive long and narrow hydrophobic channel (*8*, *19*). Notably, a number of acyl lysine–competitive small-molecule and peptidomimetic inhibitors have been developed (*27*–*37*). However, the structural and sequence similarity between ENL and AF9 YEATS domains poses challenges in achieving selectivity. To date, most of the reported inhibitors have exhibited comparable affinities for both ENL and AF9 YEATS domains. Recently, our laboratory developed a small-molecule inhibitor with strong selectivity for the ENL YEATS domain (*32*).

Proteolysis targeting chimeras (PROTACs) are a class of heterobifunctional small molecules that engage a target protein with an E3 ubiquitin ligase complex, thereby instigating ligand-dependent protein degradation at the proteasome (*38*). This technology has generated substantial interest in both the biomedical and drug discovery communities. While prior research on conventional occupancy-driven ENL YEATS small-molecule inhibitors has provided a foundation for the development of ENL PROTAC degraders, progress in this area has been limited. To date, only two thalidomide-based ENL degraders, which recruit the cereblon (CRBN) E3 ligase, have been reported (*31*, *39*). However, thalidomide-based PROTACs are known to have a common issue of off-target degradation of neo-substrates such as IKZF1/3, transcription factors with important role in hematological cells (*31*, *40*, *41*). Another neo-substrate, GSPT1, a translation termination factor, is probably the

[1]Department of Epigenetics, Van Andel Institute, Grand Rapids, MI, USA. [2]Mount Sinai Center for Therapeutics Discovery, Departments of Pharmacological Sciences, Oncological Sciences, and Neuroscience, Tisch Cancer Institute, Icahn School of Medicine at Mount Sinai, NY, New York, USA. [3]Department of Biochemistry and Biophysics, University of North Carolina at Chapel Hill, Chapel Hill, NC, USA.
*Corresponding author. Email: hong.wen@vai.org (H.W.); jian.jin@mssm.edu (J.J.)
†These authors contributed equally to this work.

most concerning neo-substrate, which may be degraded by CRBN-recruiting PROTACs because of the critical role of GSPT1 in most cells and potential toxic caused by its degradation (*42*). Therefore, further efforts are needed to explore diverse designs of ENL PROTAC molecules that overcome these limitations and offer improved selectivity and safety profiles.

In this study, we have developed MS41, a highly potent, selective, and in vivo efficacious ENL PROTAC degrader that recruits the von Hippel–Lindau (VHL) E3 ubiquitin ligase. MS41 potently and selectively induces the degradation of ENL through the ubiquitin-proteasome pathway. MS41 effectively inhibits leukemia cell proliferation and clonogenic ability in vitro and suppresses leukemia progression in a xenograft mouse model of *MLL*-r leukemia in vivo. Mechanistically, MS41-induced ENL degradation leads to reduced chromatin occupancy of ENL-associated transcription machinery, resulting in the suppression of key oncogenic gene expression programs that are essential for tumor maintenance. In addition, MS41 exhibits no detectable in vivo toxicity. It exerts only mild effects on normal hematopoiesis, with these changes being fully reversible upon treatment cessation. Together, our findings highlight the potential of pharmacological ENL degradation as a promising therapeutic strategy for ENL-dependent cancers. We provide MS41 to the biomedical community as not only a valuable in vivo chemical probe but also a promising anticancer therapeutic.

RESULTS

MS41 is a potent ENL PROTAC degrader

In our pursuit to develop effective ENL PROTAC degraders, we used PFI-6, one of the most potent ENL/AF9 YEATS inhibitors (*36*), and VHL1 and VHL1-Me, two classic ligands of the VHL E3 ubiquitin ligase (*43*, *44*), for compound design (Fig. 1, A to C, and fig. S1). The cocrystal structure of PFI-6 in complex with the AF9 YEATS domain (PDB code: 8PJ7) (*36*) revealed that the inhibitor binds to the Kac-binding site with both ends of the compound solvent exposed, making it suitable for linker attachment to design PROTACs (Fig. 1B). We chose the right-hand side dihydro indene group and modified its phenyl ring (Fig. 1B) with a carboxylic acid functionality to attach various linkers connected to VHL ligands (Fig. 1C and fig. S1). To screen compounds for their ability to induce ENL protein degradation in cells, we stably expressed 3Flag–hemagglutinin (HA)–tagged ENL (3Flag-HA-ENL) in the human *MLL*-r leukemia cell line MV4;11 and monitored ENL protein levels via Western blot analysis. We began by testing different types of linkers, including polyethylene glycol (PEG) linkers (compounds **1** to **4**) and carbon linkers of varying lengths (compounds **5** to **12**) (fig. S1). We observed that, when treating cells at 1 and 10 μM for 24 hours, none of the compounds with PEG linkers induced substantial ENL degradation (fig. S2A). Compounds with short carbon linkers (compounds **5** to **7**, with linkers ranging from 2C to 6C) also did not exhibit strong effect. However, the ENL degradation effect became more pronounced with longer carbon linkers (compounds **8** to **12**, with linkers ranging from 7C to 11C) (fig. S2A). Next, since compounds with long carbon linkers (compounds **10** to **12**, 9C to 11C) induced effective ENL degradation, we designed and synthesized corresponding analogs (compounds **13** to **15**, 9C to 11C) (fig. S1) by replacing VHL1 with VHL1-Me as the VHL binder, which has higher binding affinity to VHL and was previously reported to result in more effective degraders (*45*–*47*). Compared to their unmethylated counterparts, the VHL1-Me compounds induced even stronger ENL protein degradation (fig. S2A). As expected, the parental ENL ligand PFI-6 could not reduce ENL protein levels (fig. S2A).

We next assessed whether these compounds could efficiently degrade endogenous ENL. To do this, we treated MV4;11 cells with compounds **10** to **15** at a wide range of concentrations (1 nM to 10 μM) for 6 and 24 hours. We found that all the tested compounds efficiently induced ENL protein degradation in a concentration-dependent manner (Fig. 1D and fig. S2, B to D). Considering the efficiency of ENL degradation and molecular weight of compounds, we chose to focus on compound **13** and renamed it as **MS41** (Fig. 1C and fig. S1). We also developed **MS41N** as a negative control of MS41. MS41N contains the same ENL-binding moiety and linker as MS41 but uses the (2*R*,4*S*) diastereoisomer of VHL1-Me that cannot bind the VHL E3 ligase (Fig. 1C) (*46*, *48*). As expected, MS41N, the same as the parental ENL ligand PFI-6, did not induce ENL degradation, even at 10 μM (Fig. 1D and fig. S2B).

MS41 consistently induced robust ENL degradation in a variety of human leukemia cell lines (Fig. 1E and fig. S2E). The half protein degradation concentration (DC_{50}) values of MS41 were measured to be 3.50, 2.84, 3.03, and 26.58 nM in MV4;11, SEMK2, Jurkat, and KASUMI1, respectively, with a maximum degradation (D_{max}) > 93% (Fig. 1F and fig. S2F). In addition, MS41 induced ENL protein degradation rapidly. When cells were treated with 100 nM of MS41, ENL degradation was observed as early as 30 min after treatment, with maximal protein degradation occurring around 6 hours (Fig. 1G and fig. S2G). Together, these results demonstrate that MS41 is a highly potent ENL PROTAC degrader.

MS41 induces ENL protein degradation through the UPS

We next determined the mechanism of action underlying MS41-induced ENL degradation. MS41, as well as MS41N, binds to the ENL YEATS domain with affinities comparable to that of PFI-6. In an AlphaScreen assay that detects the ENL YEATS–H3K9ac interaction (*32*), the half-maximal inhibition concentrations (IC_{50}) of MS41, MS41N, and PFI-6 were measured at 119.43, 117.43, and 69.81 nM, respectively (fig. S2H). Pretreatment of MV4;11 cells with PFI-6 inhibited MS41-mediated ENL degradation in a concentration-dependent manner (Fig. 2A), confirming that the induction of ENL protein degradation by MS41 is an on-target effect. Similarly, pretreatment of cells with the VHL ligand VH298 (*49*) also hindered MS41-mediated ENL degradation (Fig. 2B). Furthermore, MS41-induced ENL degradation was effectively blocked by pretreating MV4;11 cells with the proteasome inhibitor MG132 or neddylation inhibitor MLN4924 (Fig. 2, C and D). In addition, CRISPR-Cas9–mediated genetic ablation of VHL in MV4;11 cells completely abolished MS41-induced ENL degradation (Fig. 2E). These findings collectively establish that MS41 is a bona fide PROTAC ENL degrader that degrades ENL in a VHL- and ubiquitin-proteasome system (UPS)–dependent manner. Furthermore, a washout experiment revealed that ENL protein levels substantially rebounded around 6 hours and were nearly fully restored approximately 12 hours after compound removal (Fig. 2F), demonstrating that MS41-induced ENL degradation is reversible.

MS41 selectively degrades ENL in leukemia cells

Within the human genome, four proteins contain YEATS domains: ENL, AF9, GAS41, and YEATS2 (*20*). ENL and AF9 are paralogous, sharing a similar protein structure, including a highly conserved

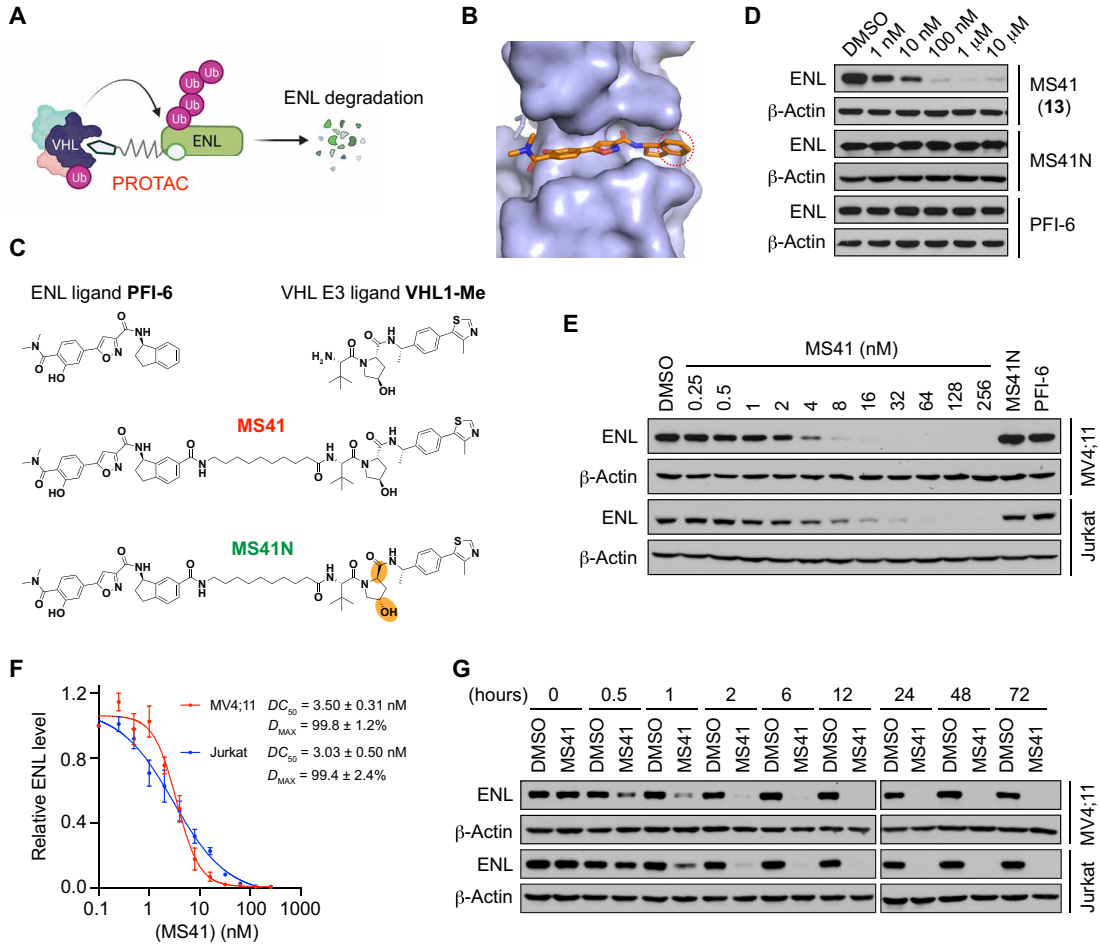

Fig. 1. Discovery of a first-in-class, highly potent VHL-recruiting ENL PROTAC degrader, MS41. (**A**) Schematic depiction of VHL-recruiting PROTAC degrader–mediated ENL degradation. Figure was created with BioRender. (**B**) Cocrystal structure of the AF9 YEATS domain (light blue) in complex with PFI-6 (orange) (PDB code: 8PJ7). The phenyl ring of PFI-6 dihydro indene group (red circle) reaches out to the binding pocket and is solvent exposed. (**C**) Chemical structures of ENL ligand PFI-6, VHL E3 ligand VHL1-Me, ENL degrader MS41, and MS41N, a negative control compound of MS41. The changed stereocenters are highlighted in orange in MS41N. (**D**) Immunoblots for ENL in MV4;11 cells treated with DMSO or the indicated concentrations of MS41 (compound **13**), MS41N, or PFI-6 for 6 hours. β-Actin was used as a loading control. (**E**) Concentration-dependent ENL degradation mediated by MS41. Immunoblots for ENL and β-Actin in MV4;11 and Jurkat cells treated with DMSO, the indicated concentrations of MS41, MS41N (256 nM), or PFI-6 (256 nM) for 24 hours. (**F**) Measurement of DC_{50} and D_{max} values of MS41 in MV4;11 and Jurkat cells. The band intensity in (E) was determined by ImageJ software. Values and error bars are presented as means ± SEM from three independent experiments. (**G**) Time-dependent ENL degradation mediated by MS41. Immunoblots for ENL in MV4;11 and Jurkat cells treated with DMSO or MS41 (100 nM) for the indicated time. β-Actin was used as a loading control. All immunoblots are representative of three biological repeats.

YEATS domain. Most ENL/AF9 YEATS domain inhibitors reported to date, such as PFI-6, cannot differentiate between ENL and AF9. In our AlphaScreen assays, which include all four human YEATS domains, we observed that, similar to PFI-6 (*36*), MS41 exhibited comparable binding affinities to ENL and AF9 YEATS domains. In contrast, no binding was detected to GAS41 or YEATS2 YEATS domains (with $IC_{50} > 50$ μM) (fig. S3A). Consistent with these results, MS41 efficiently degraded both ENL and AF9 in a concentration-dependent manner in cells, whereas it had no effect on GAS41 and YEATS2 protein levels, even at a concentration of 1 μM (Fig. 2G). In this experiment, the degradation of AF9 was monitored in cells stably expressing 3Flag-HA–tagged AF9 protein, as the endogenous AF9 is expressed at very low levels in MV4;11 cells, undetectable by Western blot.

To further assess the selectivity of MS41 on a proteome-wide scale, we conducted unbiased mass spectrometry (MS)–based global proteomic analyses on MV4;11 cells treated with MS41, MS41N, or the dimethyl sulfoxide (DMSO) control. Cells were treated for 2 or 6 hours, and the degradation of ENL by MS41 was confirmed by Western blot before MS analysis (fig. S3B). At both time points, of the 4494 proteins detected with ≥2 RazorUnique peptides, only ENL exhibited a profound reduction in abundance when treated with MS41 relative to the DMSO or MS41N treatment (with a cutoff of P value <0.05 and fold change >1.5) (Fig. 2H, fig. S3C, and table S1). In contrast, MS41N did not substantially alter the abundance of any proteins compared to the DMSO control (fig. S3D and table S1). Together, these results strongly demonstrate that MS41 is a highly selective ENL degrader.

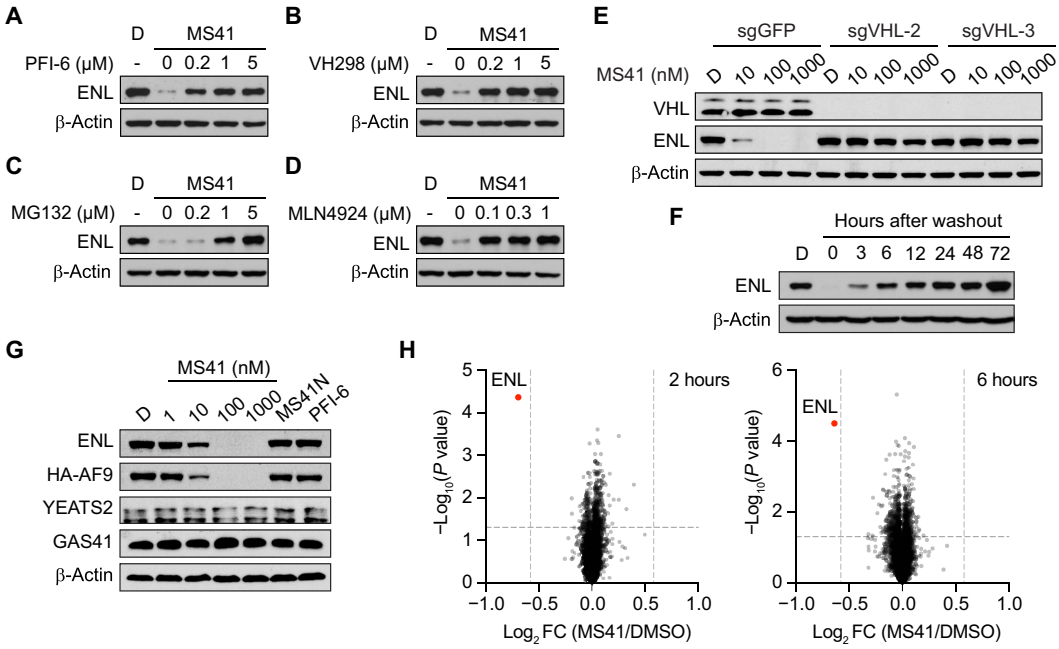

Fig. 2. MS41 selectively induces ENL protein degradation in human leukemia cells through the UPS. (**A** to **D**) Immunoblots for ENL in MV4;11 cells pretreated with the indicated concentrations of PFI-6 (A), VHL ligand VH298 (B), proteasome inhibitor MG132 (C), or neddylation inhibitor MLN4924 (D) for 1 hour, followed by a 2-hour treatment with 100 nM MS41. D, DMSO. (**E**) Immunoblots for VHL and ENL in MV4;11 cells expressing a control sgRNA (sgGFP) or VHL sgRNAs treated with the indicated concentrations of MS41 for 24 hours. (**F**) Immunoblots for ENL in MV4;11 cells pretreated with 100 nM MS41 for 24 hours, followed by washout for the indicated time. (**G**) Immunoblots for endogenous ENL, GAS41, and YEATS2 and ectopically expressed HA-AF9 in MV4;11 cells treated with the indicated concentrations of MS41, MS41N (1 μM), or PFI-6 (1 μM). Immunoblots in (A) to (G) are representative of three independent experiments. β-Actin was used as a loading control. (**H**) Quantitative proteomics analysis of MV4;11 cells treated with 100 nM MS41 versus DMSO for 2 or 6 hours. A total of 4994 proteins were identified with ≥2 RazorUnique peptides and quantified. The dash lines indicate a cutoff of *P* value <0.05 (*y* axis) and fold change >1.5 (*x* axis) in three biological replicates.

MS41 exhibits potent inhibition of leukemia cell survival

Previous studies have demonstrated that genetic depletion of ENL leads to growth inhibition in human acute leukemia cells, particularly in *MLL*-r leukemia cells (*7*, *8*). Therefore, we assessed the antiproliferative effects of MS41 in a panel of human leukemia cell lines. The impact of MS41 treatment mimicked the effects of ENL knockout (KO) in several *MLL*-r leukemia cell lines containing MLL-AFF1 fusions, including MV4;11, RS4;11, and SEMK2, whereas MS41N or PFI-6 did not suppress cell growth (Fig. 3, A to C). The half-maximal growth inhibition concentration (GI_{50}) values of MS41 in MV4;11 and RS4;11 cells were measured to be 21.28 and 25.06 nM, respectively (Fig. 3D), underscoring the high potency of MS41 in inhibiting cell growth. MS41 also suppressed cell growth in leukemia cell lines harboring other MLL fusions, such as OCI-AML2 and ML-2 with MLL-AF6 fusions and NOMO-1 with MLL-AF9 fusion (fig. S4, A and B). KASUMI1, a leukemia cell line harboring the *AML1-ETO* translocation, was also sensitive to MS41, with a GI_{50} of 69.05 nM (Fig. 3, A and D). In contrast, MS41 had no or minimal effects on growth inhibition (GI_{50} > 50 μM) in Jurkat and K-562, two non–*MLL*-r leukemia cell lines that are insensitive to ENL KO (Fig. 3, A and D, and fig. S4, A and B).

Next, we evaluated the impact of MS41 on the clonogenic potential of leukemia cells by colony formation cell assays. The results revealed that MS41, but not MS41N or PFI-6, impaired the clonogenic potential of several ENL-sensitive leukemia cells, including MV4;11, SEMK2, and KASUMI1 (Fig. 3, E and F, and fig. S4, C and D). Notably, MS41 not only substantially reduced colony numbers but also greatly decreased the size of the colonies and altered colony morphology (Fig. 3E). In contrast to these ENL-dependent cells, MS41 had no discernible impact on the colony formation of Jurkat cells (fig. S4, E and F). To investigate how MS41 inhibits leukemia cell survival, we examined changes in cell cycle and apoptosis in MV4;11 cells. The results showed that MS41 induced G_1 cell cycle arrest and increased apoptosis in a time-dependent manner, while MS41N or PFI-6 had no such effects (Fig. 3, G and H). Collectively, these results demonstrate that MS41 exhibits superior activity compared to its parental ENL ligand, PFI-6, in inhibiting leukemia cell survival.

Furthermore, we assessed the cotreatment of MV4;11 cells with MS41 and doxorubicin, a commonly used chemotherapy agent in AML treatment, and observed a strong synergistic effect between the two. With 10 nM doxorubicin, the GI_{50} of MS41 decreased from 21.5 to 7.35 nM (fig. S4, G and H), indicating promising therapeutic potential for this combinatorial treatment.

MS41 suppresses key oncogenic gene expression programs in leukemia cells

To investigate the molecular mechanism by which MS41 inhibits leukemia cell growth, we performed RNA sequencing (RNA-seq) analysis in MV4;11 cells treated with MS41, MS41N, PFI-6, or DMSO. RNA samples were collected at two time points after treatment: 6 hours (an early time point when more than 90% of ENL proteins were depleted) and 24 hours (before noticeable phenotypic changes occurred). The depletion of ENL proteins by MS41 was confirmed by Western blot analysis (fig. S5A). At 6 hours after MS41

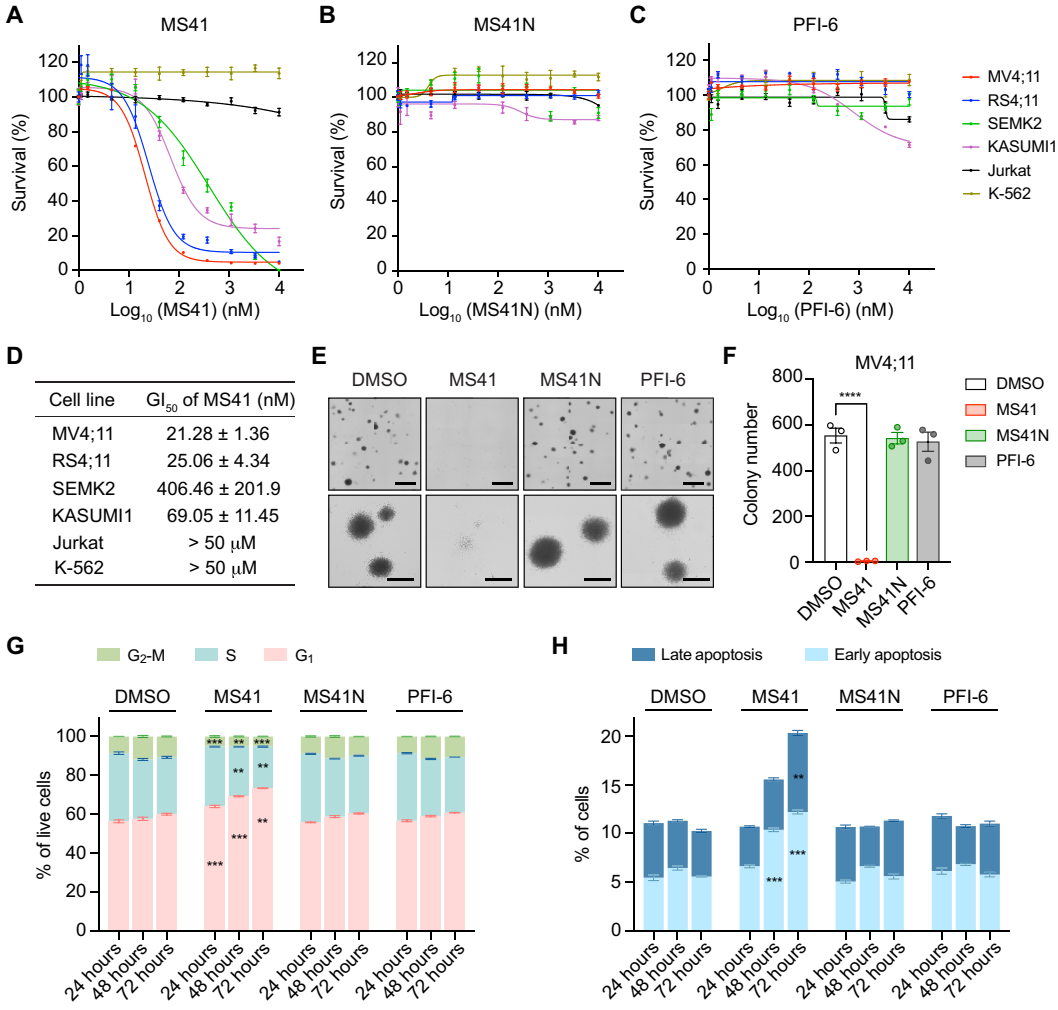

Fig. 3. MS41 displays potent growth inhibitory activity in human leukemia cells. (**A** to **C**) Growth inhibition curves of MS41 (A), MS41N (B), and PFI-6 (C) in human leukemia cells, MV4;11, RS4;11, SEMK2, KASUMI1, Jurkat, and K-562. *Y* axis shows the relative live cell ratio upon treatment with the indicated concentrations (*x* axis) of compound for 6 days, normalized to DMSO-treated cells. Error bars represent means ± SEM from three independent experiments. (**D**) Table of GI_{50} comparison of MS41 in MV4;11, RS4;11, SEMK2, KASUMI1, Jurkat, and K-562 cells. (**E** and **F**) Representative images (E) and quantification (F) of colonies formed in MV4;11 cells treated with DMSO, 100 nM of MS41, MS41N, or PFI-6 for 10 days. Scale bars, 2 mm (top) and 500 μm (bottom). (**G** and **H**) Cell cycle profile (G) and apoptotic analysis (H) of MV4;11 cells treated with DMSO, 100 nM of MS41, MS41N, or PFI-6 for the indicated time. In (F) to (H), error bars represent means ± SEM from three independent experiments. Student's *t* test, compared with DMSO treatment at corresponding time points, $^{**}P < 0.01$, $^{***}P < 0.001$, $^{****}P < 0.0001$.

treatment, compared to cells treated with DMSO, we detected only 123 genes down-regulated and 463 genes up-regulated [fold change > 1.5, false discovery rate (FDR) < 0.05] (fig. S5B and table S2). By 24 hours, we identified more differentially expressed genes (DEGs), with 741 genes down-regulated and 1450 genes up-regulated (Fig. 4A, fig. S5B, and table S2). In contrast, MS41N or PFI-6 did not induce substantial changes in gene expression (fig. S5B and table S2). Volcano plots revealed that the expression of key oncogenes (e.g., *MYC*) and leukemia stem cell (LSC) genes (e.g., *HOXA9*, *HOXA10*, *MEIS1*, and *MYB*) was greatly reduced, while the expression of myeloid differentiation markers (e.g., *CD11B* and *CD11C*) increased in MS41-treated cells compared with DMSO-treated cells (Fig. 4, B and C). Furthermore, reverse transcription quantitative polymerase chain reaction (RT-qPCR) validated concentration-dependent gene expression changes induced by MS41 in cells treated with MS41, but not by MS41N or PFI-6 (Fig. 4D). We also confirmed that MS41 as well as MS41N and PFI-6 did not affect mRNA levels of ENL (fig. S5C).

To ascertain whether MS41-induced gene expression changes are due to the on-target effect of ENL depletion, we also performed RNA-seq analysis in MV4;11 cells with ENL knocked out via CRISPR-Cas9 editing. We used two ENL single-guide RNAs (sgRNAs) (*8*), both of which reduced ENL proteins by >90% (fig. S5D). RNA-seq analysis identified 108 genes down-regulated and 561 genes up-regulated in ENL KO cells (fig. S5B and table S3). Gene set enrichment analyses (GSEA) (*50*) and correlation analyses unveiled that gene expression changes induced by MS41-mediated ENL degradation were consistent with gene expression changes observed in ENL KO cells (Fig. 4E and fig. S5, E to G). We also observed correlated gene expression changes in MV4;11 cells with ENL degradation induced by MS41 or by dTAG-13 in an engineered dTAG/ENL system (fig. S5, H and I) (*7*). MS41 treatment resulted in down-regulation of MYC-associated

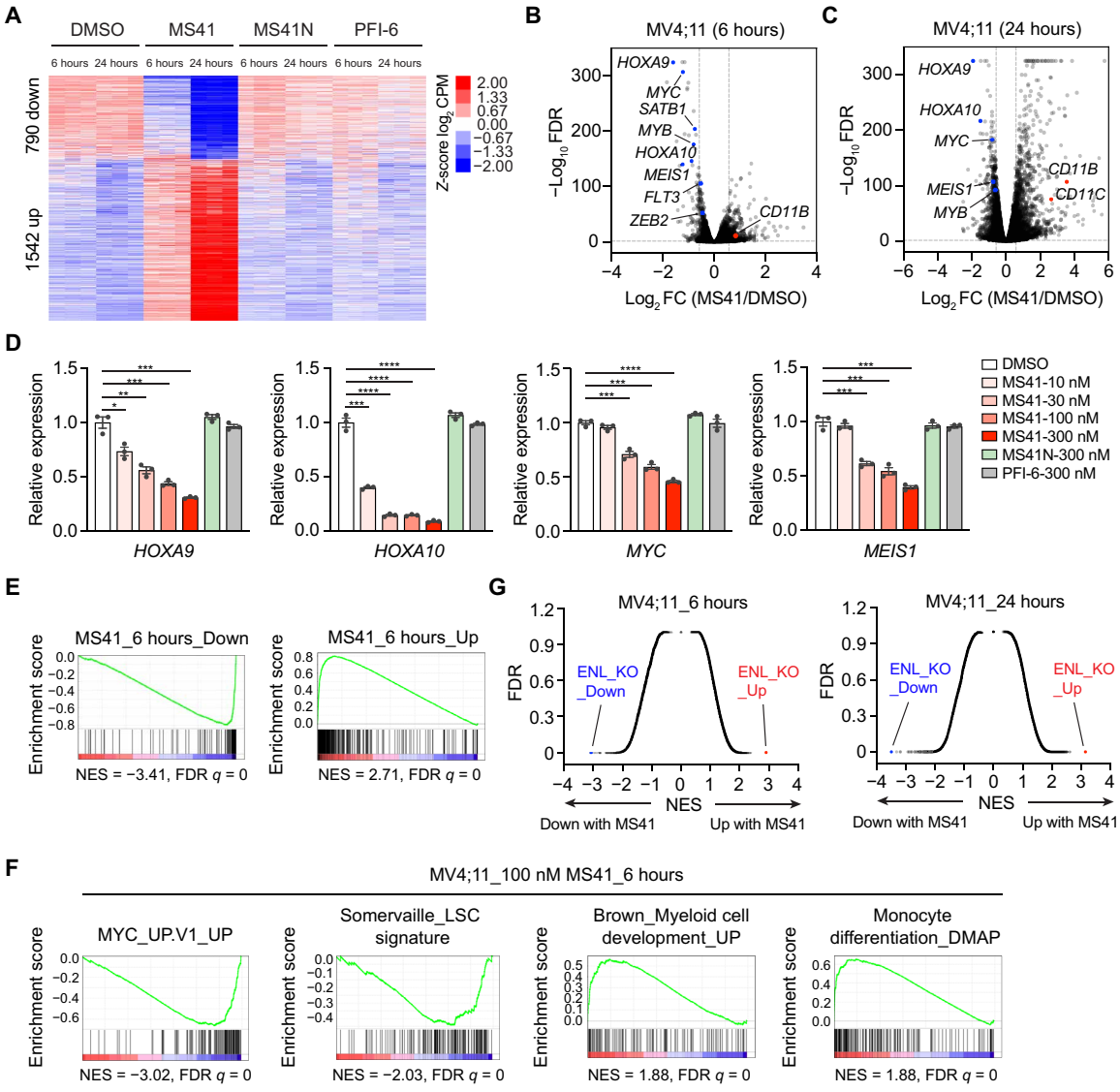

Fig. 4. MS41 suppresses ENL-dependent oncogenic gene expression programs. (**A**) Heatmap representation of DEGs from MS41 versus DMSO-treated MV4;11 cells. $n = 3$ biological replicates. CPM, counts per million. (**B** and **C**) Volcano plots of all expressed genes in MV4;11 cells after MS41 treatment for 6 hours (B) and 24 hours (C). The *x* axis is $\log_2$ fold change ($\log_2$ FC) of CPM values from MS41 versus DMSO. The *y* axis is $-\log_{10}$ transformed FDR values for each gene. Key down genes are highlighted in blue and up genes in red. (**D**) RT-qPCR analysis showing mRNA expression levels of selected ENL target genes in MV4;11 cells treated with DMSO or the indicated concentrations of MS41, MS41N, or PFI-6 for 24 hours. Error bars represent means ± SEM from three independent experiments. Student's *t* test, $^*P < 0.05$, $^{**}P < 0.01$, $^{***}P < 0.001$, $^{****}P < 0.0001$. (**E**) GSEA plots with ENL KO as ranking list and Down (left) and Up (right) DEGs of 6-hour MS41 treatment as gene sets. NES, normalized enrichment score. (**F**) GSEA plots with 6-hour MS41 versus DMSO in MV4;11 as ranking list and the selected curated gene sets. (**G**) *X*-*y* plots of GSEA results with 6 or 24 hours MS41 versus DMSO in MV4;11 cells as ranking list and human MSigDB C2 as gene sets. *X* axis is NES values; *y* axis is corresponding FDR values.

gene expression, LSC signature (*51*), and a gain of myeloid cell development and monocyte differentiation signatures (Fig. 4F, fig. S5J, and table S4), aligning with the known roles of ENL in regulating LSC functions (*7*, *8*). Furthermore, we compared MS41-induced DEGs against >6000 curated gene sets in the Molecular Signatures Database (MSigDB) (*52*) and identified ENL-dependent gene sets among the most enriched upon MS41 treatment (Fig. 4G), underscoring the specific on-target effect of MS41.

We also performed RNA-seq analysis in another *MLL*-r cell line, SEMK2. MS41 treatment for 24 hours completely depleted ENL proteins in SEMK2 cells (fig. S5K). We identified only a small number of DEGs (<100) in MS41-treated SEMK2 cells. Nevertheless, key LSC genes, such as *HOXA9* and *HOXA10*, were among the most substantially down-regulated genes (fig. S5L and table S5). Similar to our observations in MV4;11 cells, GSEA revealed that MS41 also induced down-regulation of MYC-associated gene expression, embryonic stem cell core genes, and LSC signature in SEMK2 cells (fig. S5M). Together, these results demonstrate that MS41 specifically suppresses ENL-dependent oncogenic gene expression programs in leukemia cells.

MS41 reduces chromatin occupancy of ENL-associated transcription elongation machinery

ENL exerts its function in transcriptional regulation through interacting with multiple chromatin-associated protein complexes, particularly the SEC and H3K79 methyltransferase DOT1L complex (*9*–*18*). Both complexes are implicated in *MLL*-r leukemia, and previous studies, including ours, have shown that the wild-type ENL plays a critical role recruiting these complexes to chromatin (*7*, *8*). To investigate whether MS41 treatment affects chromatin occupancy of ENL-associated transcription machinery, we performed chromatin immunoprecipitation coupled with next-generation sequencing (ChIP-seq) for components of the SEC and DOT1L complexes. For this, we used the same treatment conditions as for the RNA-seq experiments (100 nM MS41, 6 hours), during which ENL was greatly depleted while other complex components remained largely unchanged (Fig. 5A). Notably, longer treatment (24 hours) led to reduced protein stability of two ENL-interacting proteins, DOT1L and AFF1. Nevertheless, no global changes were detected in active epigenetic marks, including H3K79me2/3, H3K4me3, H3K9ac, and H3K27ac (Fig. 5A and fig. S6A). ChIP-seq using an anti-ENL antibody in MV4;11 cells identified approximately 2500 genes with ENL ChIP-seq signals, all of which were completely diminished upon MS41 treatment (Fig. 5, B and C, and table S6). Consistent with previous reports (*7*, *8*), ENL primarily occupied gene promoters and exhibited skewed bindings on target genes, with strong binding observed on only a small portion of the target genes (Fig. 5, B and C). On the basis of the rank-ordered ENL-binding density, we divided ENL target genes into two groups: those with high (134 genes) and low (2375 genes) ENL bindings (Fig. 5C). Notably, most genes with the greatest down-regulation upon MS41 treatment fell in the high ENL–bound group, including key leukemia oncogenic genes such as *HOXA9*, *MEIS1*, *MYB*, *SATB1*, and *BAHCC1*. Compared to the non- and low ENL–bound genes, ENL occupancy on the high ENL–bound genes was reduced the most by MS41 treatment (Fig. 5D), suggesting that genes with high ENL occupancy are likely more functionally relevant.

Next, we performed ChIP-seq for components of the SEC (AFF1 and CDK9), DOT1L, and elongating RNA polymerase (Pol II S2P) in the same cells treated with MS41. Chromatin occupancies of the SEC and DOT1L complex components, as well as the elongating Pol II, were highly correlated with ENL occupancy, with higher binding densities observed on the high ENL–bound genes (Fig. 5, E to H). Their chromatin occupancies were all reduced upon MS41 treatment, with the most prominent reductions observed on the high ENL–bound genes (Fig. 5, E to H, and fig. S6B). In line with these changes, the high ENL–bound genes showed a greater reduction in gene expression induced by MS41 (Fig. 5I). The positive correlations of chromatin occupancies of ENL and ENL-associated complexes with gene expression were more evident on key ENL target genes such as *HOXA9*, *HOXA10*, *MEIS1*, and *MYB* (Fig. 5J).

DOT1L regulates transcription elongation by modulating H3K79 methylation (*15*, *16*). Because of the low turnover rate of this modification, we performed ChIP-seq for H3K79me2 at 24 hours after MS41 treatment. Consistent with DOT1l occupancy, H3K79me2 levels were positively correlated with ENL occupancy (fig. S6, C and D). Moreover, upon MS41 treatment, H3K79me2 levels decreased on the high ENL–bound genes, including the key ENL target genes (fig. S6, D and E) but was not substantially changed on non-ENL–bound genes. Similar patterns were also observed for two other active marks, H3K27ac and H3K4me3 (fig. S6, F and G). Collectively, these results demonstrate that MS41 suppresses gene expression by reducing the chromatin occupancy of ENL-associated transcription machinery and related active epigenetic marks on target genes.

MS41-induced degradation of ENL is reversible (Fig. 2F). Similarly, DOT1L and AFF1 were fully recovered 24 to 48 hours after washout (fig. S7A). Furthermore, the expression of ENL target genes, including *HOXA9*, *HOXA10*, *MYC*, and *MEIS1*, was also recovered after removal of MS41 (fig. S7B). The mRNA level of ENL itself was not affected by MS41 treatment or the subsequent washout. Together, these results demonstrate the reversible effects of MS41 in cells.

MS41 suppresses leukemia progression in vivo

Motivated by the robust effect of MS41 in inhibiting leukemia cell survival in vitro, we aimed to assess the therapeutic potential of ENL degradation in animal models. In our in vivo studies, we first evaluated the pharmacokinetic (PK) properties of MS41 in mice. After a single intraperitoneal (i.p.) injection at a dose of 50 mg/kg, the maximum plasma concentration of MS41 reached 241.8 nM, and the concentration retained above 30 nM for approximately 24 hours (Fig. 6A). MS41 was well tolerated by mice, with no clinical signs observed in our PK study. Given that the GI_{50} of MS41 in MV4;11 cells is less than 30 nM, we used intravenous MV4;11 xenografts as a model of *MLL*-r leukemia and opted for a daily intraperitoneal dosing regimen of 50 mg/kg of MS41 for in vivo efficacy studies.

For the xenograft model, NOD *scid* gamma (NSG) mice were irradiated at a sublethal dose [2 gray (Gy)] and subsequently transplanted with MV4;11 cells via tail vein injection. These MV4;11 cells were engineered to stably express turboGFP and luciferase, enabling the monitoring of engraftment through bioluminescent imaging (BLI). Ten days after transplantation, engraftment was confirmed by BLI, and mice were randomly divided into two groups: one receiving MS41 treatment and the other with a vehicle control (Fig. 6B). In a survival study, all mice in the vehicle cohort ($n = 11$) succumbed to the disease within 42 days after transplantation, whereas the mice in the MS41 treatment cohort ($n = 12$) exhibited delayed disease progression and prolonged survival. The median survival was 49.5 days for the MS41 group compared to 37 days for the vehicle group (Fig. 6C). MS41 treatment did not lead to any noticeable body weight loss during the course of the treatment.

We measured percentage of human $CD45^+$ ($hCD45^+$) cells (MV4;11 cells) in peripheral blood (PB) to monitor leukemia progression. Compared to the mice in the vehicle group, mice received MS41 treatment had much lower percentage of $hCD45^+$ cells in their PB (Fig. 6D). In a separate cohort of animal study, we performed weekly BLI. The luminescence signals in mice treated with vehicle quickly escalated within 3 weeks after leukemia cell transplantation, whereas mice received MS41 treatment displayed a markedly lower leukemia burden and slower disease progression (Fig. 6, E and F). At the endpoint necropsy, we performed hematoxylin and eosin (H&E) staining and observed extensive infiltration of human leukemia cells in bone marrow, liver, and spleen of mice in the vehicle group (Fig. 6G). Ki-67 staining indicated that these leukemia cells were highly proliferative (Fig. 6H). In contrast, mice treated with MS41 had much less human leukemia cells and much fewer Ki-67–positive cells in their tissues. We also confirmed that the MS41 treatment induced complete ENL degradation by immunoblotting of leukemia cells in bone marrow of the treated mice (Fig. 6I). Collectively, these results demonstrate that MS41 is

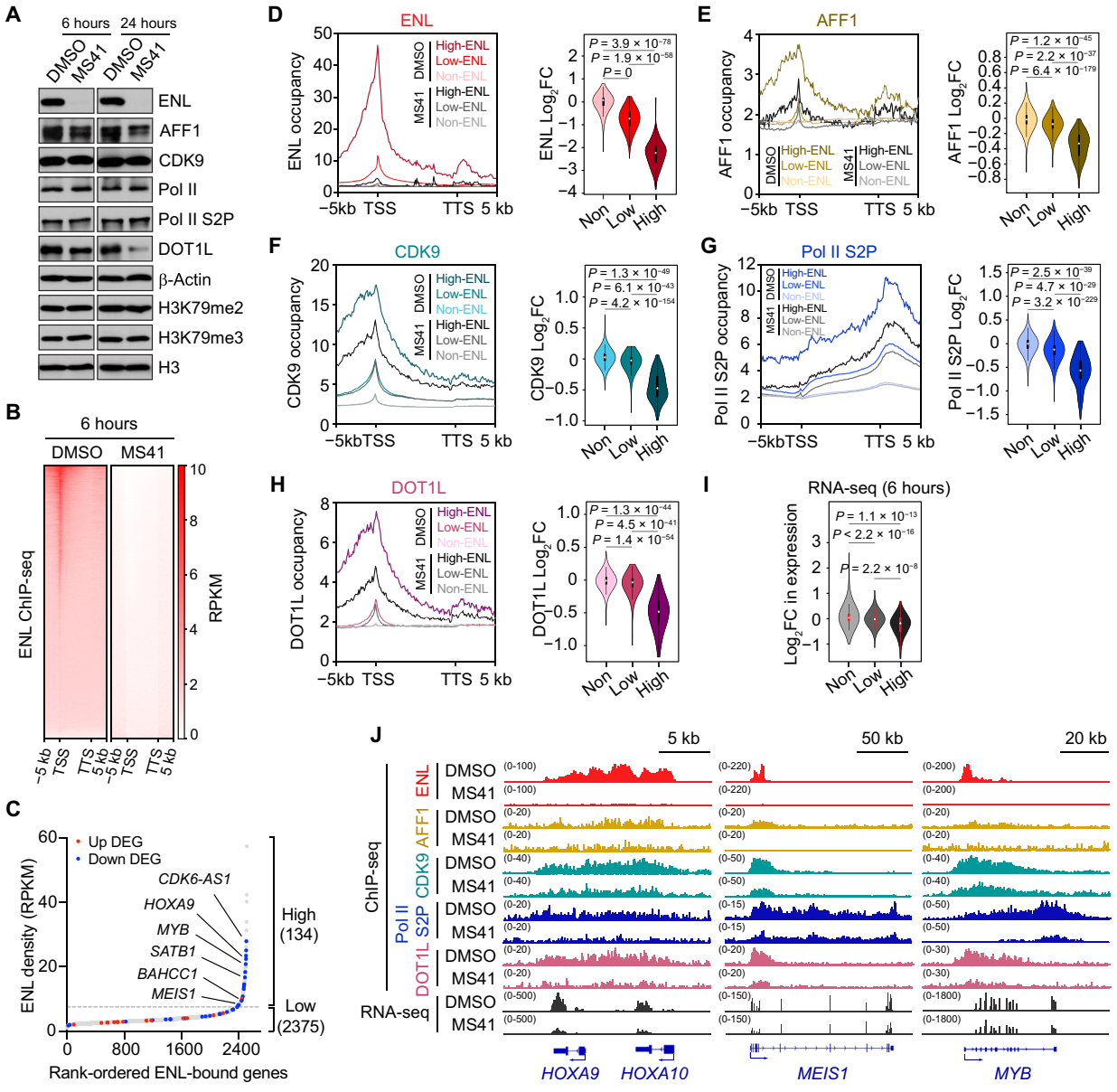

Fig. 5. MS41 reduces chromatin occupancy of ENL and its associated protein complexes. (**A**) Immunoblots for ENL, AFF1, CDK9, Pol II, Pol II S2P, DOT1L, β-Actin, H3K79me2, H3K79me3, and H3 in MV4;11 cells treated with DMSO or 100 nM MS41 for 6 and 24 hours. (**B**) Heatmaps of ENL ChIP-seq densities on all genes in MV4;11 cells treated with DMSO or 100 nM MS41 for 6 hour. $n = 3$ biological replicates. RPKM, reads per kilobase million. TSS, transcription start site; TTS, transcription termination site. (**C**) Waterfall plot of all ENL-bound genes in 6 hours DMSO sample ranked by ENL densities from low to high in *x* axis. The high and low ENL–bound genes were separated on point for which a line with a slope of 1 was tangent to the curve. Red and blue dots mark up and down DEGs, respectively, in 6-hour MS41 versus DMSO-treated cells. (**D** to **H**) Average profiles of ENL (D), AFF1 (E), CDK9 (F), RNA Pol II S2P (G), and DOT1L (H) ChIP-seq densities on high-, low-, and non-ENL–bound genes as defined in (B) and (C) (left). Violin plots of $\log_2$ fold changes ($\log_2$ FC) of corresponding ChIP-seq densities in MS41 versus DMSO from the left panel (right). Two-tailed *t* test was used for calculating *P* values. (**I**) Violin plot of $\log_2$ FC of 6-hour MS41 versus DMSO RNA-seq CPM values. Two-tailed *t* test was used for calculating *P* values. (**J**) Integrative Genomics Viewer (IGV) views of ChIP-seq densities of (D) to (H) and RNA-seq reads on *HOXA9/10*, *MEIS1*, and *MYB* genes.

efficacious in suppressing *MLL*-r leukemia progression in vivo, supporting that MS41 is a promising therapeutic for treating a subtype of leukemias that are dependent on ENL.

To determine gene expression changes induced by MS41 in vivo, we sorted hCD45$^+$ MV4;11 cells from the bone marrow of mice treated with MS41 or vehicle for 35 days and conducted RNA-seq analysis. We identified approximately 90 DEGs between MS41 and vehicle samples (fig. S8A and table S7), including key ENL targets *HOXA9* and *MYC*. GSEA revealed that down-regulated genes identified in MS41-treated MV4;11 cells in vitro were negatively enriched, whereas up-regulated genes were positively enriched, in the gene expression profiles of the xenografted cells treated with MS41 in vivo (fig. S8B). Furthermore, similar to what was observed in MV4;11 cells in vitro, MYC-associated gene expression, LSC and

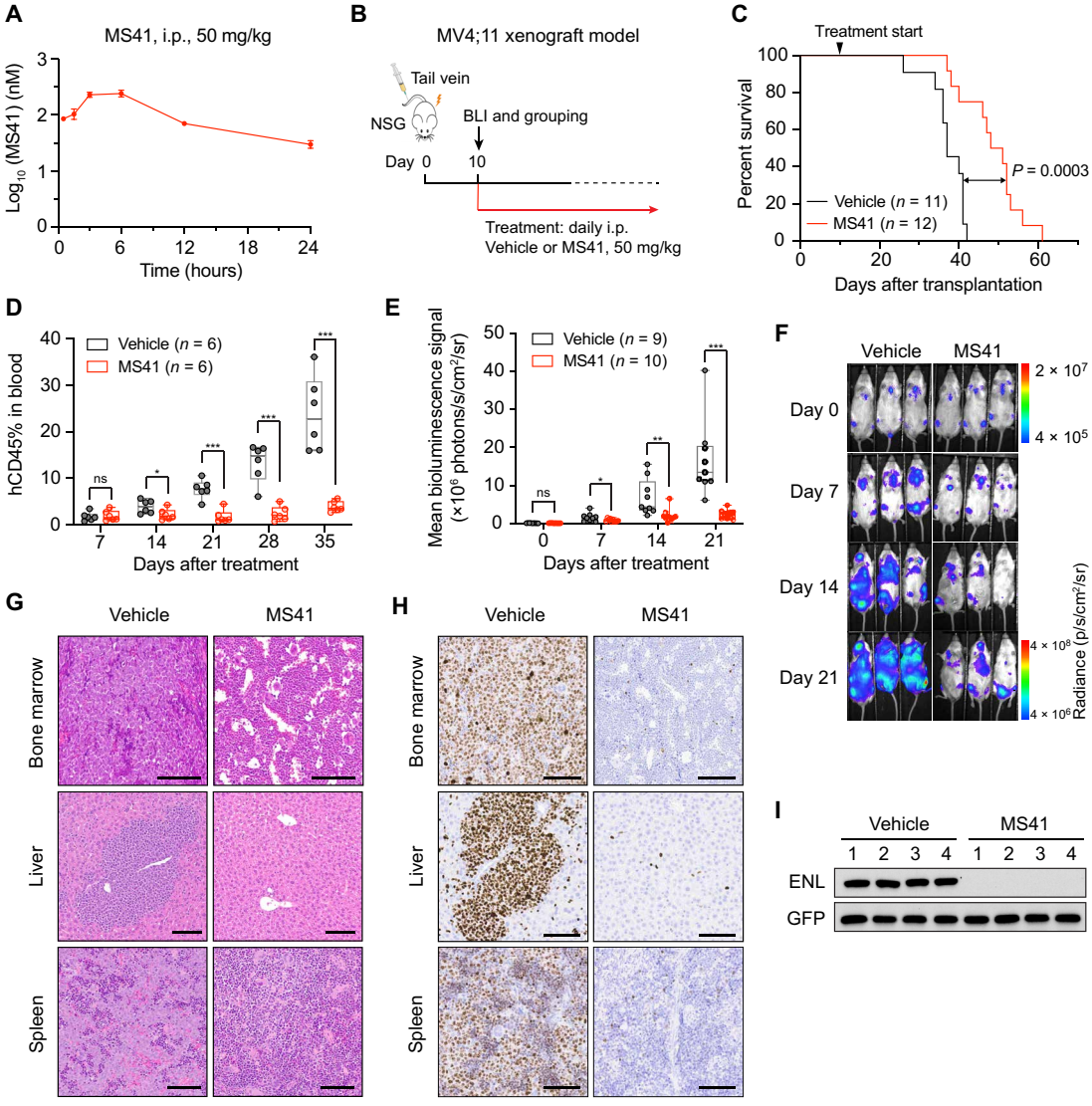

Fig. 6. MS41 suppresses leukemia progression in a xenograft model of *MLL*-r leukemia. (**A**) Plasma concentrations of MS41 over a 24-hour period in mice after a single intraperitoneal (i.p.) injection of MS41 (50 mg/kg). Error bars represent means ± SD from three mice per time point. (**B**) Schematic of the MV4;11 xenotransplantation model and treatment workflow. (**C**) Kaplan-Meier survival curves of mice treated with vehicle ($n = 11$) and MS41 ($n = 12$, 50 mg/kg, once daily, i.p.) in the xenograft model. Log-rank test was used. (**D**) Quantification of MV4;11 cells (human CD45$^+$) in the peripheral blood collected at the indicated time points from xenografted mice. Student's *t* test, $^*P < 0.05$, $^{***}P < 0.001$; ns, not significant. (**E** and **F**) Quantification of mean bioluminescence signals (E) and representative bioluminescence images (F) of xenografted mice at the indicated time points. Student's *t* test, $^*P < 0.05$, $^{**}P < 0.01$, $^{***}P < 0.001$; ns, not significant. (**G** and **H**) H&E (G) and Ki-67 immunohistochemistry (H) staining of bone marrow, liver, and spleen of moribund vehicle or MS41-treated xenografted mice. Scale bars, 100 μm. (**I**) Immunoblots for ENL and turboGFP of vehicle or MS41-treated bone marrow collected from moribund mice.

embryonic stem cell signatures, and HOXA9 target gene expression were all negatively enriched in MS41-treated leukemia cells in vivo (fig. S8C). Together, these results suggest that in vivo, MS41 works through a similar mechanism as in vitro to suppress oncogenic gene expression.

MS41 shows negligible in vivo toxicity and a mild impact on normal hematopoiesis

An integral aspect of assessing a compound's suitability for further drug development lies in its lack of in vivo toxicity. We therefore set out to assess the potential in vivo toxicity of MS41 using immune competent C57BL/6 mice. In this assessment, we treated healthy C57BL/6 mice for a consecutive 30 days, following the same regimen as used in the xenograft study (either vehicle or 50 mg/kg of MS41, i.p. administered daily) (Fig. 7A). The 30-day MS41 treatment did not induce overt toxicity or lead to evident changes in body weight (Fig. 7B). Following the completion of treatment, six mice from each group were euthanized, and the weights of various organs were measured. No significant differences were observed in most of the measured organs, including the liver, thymus, lymph nodes, heart, and kidneys, between the two treatment groups, except for a slight enlargement of the spleens in MS41-treated mice

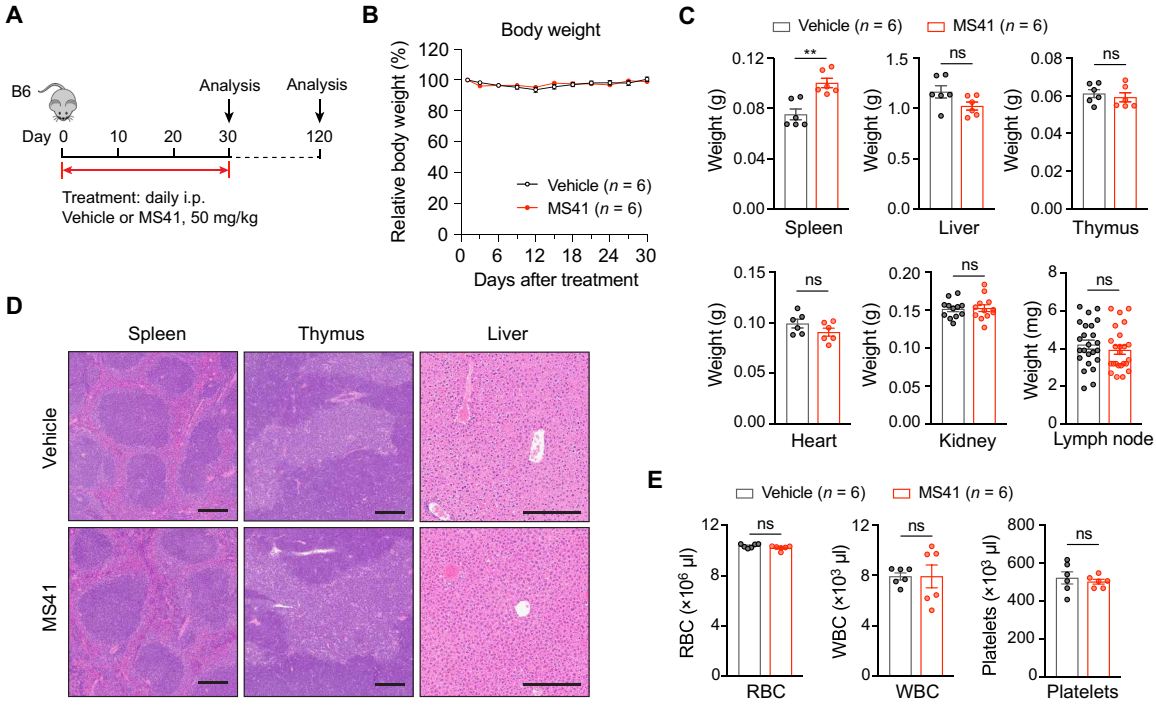

Fig. 7. MS41 exhibits no in vivo toxicity. (**A**) Schematic of MS41 treatment workflow in C57BL/6 mice. (**B**) Quantification of relative body weight over 30 days of vehicle or MS41 (50 mg/kg, once daily, i.p.) treatment. Mouse body weight was measured every 3 days. (**C**) Weight quantification of spleen, liver, thymus, heart, kidney, and lymph node collected from mice at the end of 30 days treatment with vehicle and MS41. (**D**) H&E staining of spleen, thymus, and liver from mice as described in (C). Scale bars, 250 μm. (**E**) Complete blood count analyses of WBCs, RBCs, and platelets of peripheral blood collected from mice as described in (C). Error bars represent means ± SEM ($n = 6$). Unpaired two-tailed t test was used for calculating P values in (C) and (E). $^{**}P < 0.01$; ns, not significant.

(Fig. 7C). Notably, H&E staining did not reveal any discernible pathological changes in the spleen, thymus, or liver (Fig. 7D). Furthermore, complete blood count analyses demonstrated no significant alterations in red blood cells (RBCs), white blood cells (WBC), and platelets (Fig. 7E).

To explore the impact of MS41 on normal hematopoiesis, we collected bone marrow cells from the euthanize animals at the end of treatment and profiled various hematopoietic and differentiated immune cell types by flow cytometry analysis. The total numbers of bone marrow cells isolated from mice in the two groups were found to be comparable (fig. S9A). While there was a modest decrease in the number of lineage-negative (Lin^-) hematopoietic stem/progenitor cells and megakaryocytic-erythroid progenitors in MS41-treated mice, no significant changes were observed in other types of hematopoietic stem cells or progenitor cells (fig. S9B). Analysis of differentiated cell populations in the bone marrow revealed modest increases in the numbers of monocytes and neutrophils, as well as small decreases in the numbers of B cells, $CD4^+$ and $CD8^+$ T cells, and erythrocytes, with no changes observed in natural killer cells in MS41-treated mice (fig. S9C).

To ascertain whether the mild changes in hematopoiesis induced by MS41 treatment are reversible, we monitored a cohort of mice for an additional 3 months after cessation of treatment (Fig. 7A) and analyzed their PB and bone marrow samples. No significant differences were detected between the vehicle- and MS41-treated mice in organ weights (fig. S10A), complete blood cell count (fig. S10B), total bone marrow cells (fig. S10C), and any subset of hematopoietic stem and progenitor cells (fig. S10D). Moreover, all mild changes in differentiated immune cell types observed at day 30 were fully reversed (fig. S10E). In sum, these results establish that MS41 has no detectable in vivo toxicity and only a mild effect on normal hematopoiesis, which is fully recoverable after the cessation of treatment.

MS41 potently depletes ENL protein with YEATS domain mutations

Recurrent and clustered small indel mutations in the ENL YEATS domain have been identified in Wilms' tumor, the most common pediatric kidney cancer, and AML (*53*–*55*). As demonstrated in our recent study, these hotspot mutations convey a gain of function in transcriptional control by ENL, which leads to hyperactivation of developmentally important genes and impaired cell fate decision (*56*). These mutations are primarily located in the C terminus of the YEATS domain (Fig. 8A), with the acyl-lysine–binding pocket remaining intact. We hypothesized that MS41 can also bind mutant ENL and induce protein degradation. In human embryonic kidney (HEK) 293 cells that ectopically express wild-type ENL or mutants (referred to as T1 and T3) at levels comparable to endogenous ENL, MS41 efficiently induced the degradation of both wild-type and mutant ENL in a concentration-dependent manner (Fig. 8B). Consequently, the aberrant expression of *HOXA11* and *HOXA13* genes induced by ENL mutants was markedly suppressed by MS41-mediated degradation of the mutant ENL (Fig. 8, C and D). In contrast, MS41N and PFI-6 had no or only minor effects on *HOXA11* and *HOXA13* gene expression.

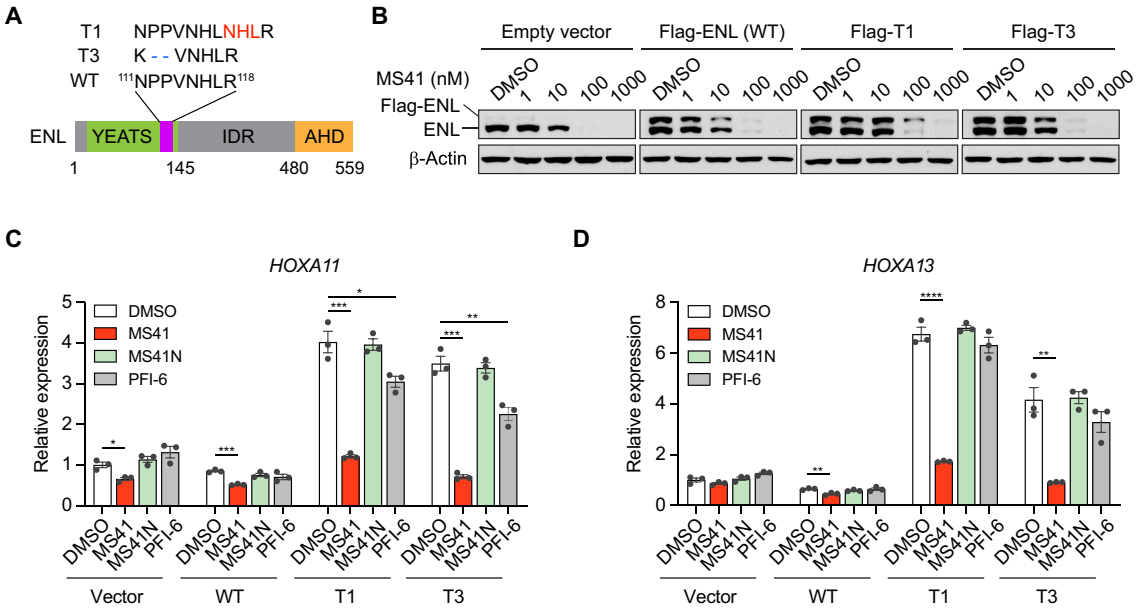

Fig. 8. MS41 potently depletes ENL protein with YEATS domain mutations. (**A**) Schematic of ENL YEATS domain mutants T1 (small insertion) and T3 (small deletion) identified in Wilms' tumor. (**B**) Immunoblots for ENL and β-actin in HEK293 cells stably expressing endogenous level of wild-type (WT) or YEATS mutant ENL (T1 and T3) treated with the indicated concentrations of MS41 for 24 hours. (**C** and **D**) RT-qPCR analysis showing mRNA expression levels of ENL target genes *HOXA11* (C) and *HOXA13* (D) in HEK293 stable cells as in (B) treated with DMSO, MS41 (100 nM), MS41N (100 nM), or PFI-6 (100 nM) for 72 hours. Error bars represent means ± SEM from three independent experiments (Student's *t* test). $*P < 0.05$, $**P < 0.01$, $***P < 0.001$, $****P < 0.0001$.

DISCUSSION

ENL has recently been identified as a critical factor in a subset of acute leukemias, particularly in *MLL*-r leukemia. It functions as a histone reader that recruits the associated SEC and DOT1L complex to chromatin through recognition of histone acylation via its YEATS domain. These studies have underscored the indispensable role of the YEATS domain (*7*, *8*, *57*). Disrupting the reader function of this domain suppresses ENL-dependent leukemia progression, suggesting that the ENL YEATS domain is a promising therapeutic target. The ENL YEATS domain contains a long and narrow hydrophobic pocket for acetyl recognition, rendering it a suitable target for developing small-molecule inhibitors. In recent years, several compounds targeting the ENL YEATS domain have been developed (*27*–*34*, *36*). These small-molecule or peptidomimetic inhibitors effectively compete with acetylated histones for binding to the hydrophobic pocket, thereby displacing ENL and its associated SEC and DOT1L complexes from chromatin and shutting down the ENL-dependent oncogenic gene expression. However, at the inception of our project, none of the reported ENL YEATS domain inhibitors had demonstrated satisfactory efficacy in suppressing leukemia cell growth or in vivo potential. This prompted us to explore an alternative strategy—the development of ENL PROTAC degraders.

One of the primary advantages of PROTACs over conventional occupancy-driven small-molecule inhibitors is their capability to completely eliminate the target protein. Moreover, the catalytic nature of PROTACs negates the need for prolonged drug exposure and high residence times, potentially resulting in more potent therapeutic effects at lower doses and with less frequent dosing, thereby minimizing side effects (*38*). In this context, MS41, the highly potent and selective ENL PROTAC degrader we developed, surpasses its parent ligand, PFI-6, in terms of inhibitory activities against leukemia cell survival. In ENL-dependent *MLL-r* cell lines such as MV4;11 and RS4;11, MS41 exhibits excellent GI_{50} (<30 nM), while PFI-6 remains ineffective even at 10 μM, a more than 300-fold increase in potency. MS41 is well-tolerated in vivo and effectively suppresses leukemia progression in a xenograft mouse model of *MLL-r* leukemia. Furthermore, MS41 exhibits no detectable in vivo toxicity. It exerts only mild effects on normal hematopoiesis, with these changes being fully reversible upon treatment cessation, suggesting a potential therapeutic window for MS41. However, despite the MS41 treatment cohort exhibiting delayed disease progression and prolonged survival, mice in this cohort died around 60 days. This may be caused by incomplete depletion of ENL in certain organs due to tissue distribution issues or potential toxicity associated with irradiation and leukemia cell transplantation in NSG mice. Nevertheless, MS41 stands as not only a valuable chemical probe but also a potential anticancer therapeutic that holds promise for further development.

During the development of MS41, two PROTAC degraders targeting ENL have been reported (*31*, *39*). SR-1114 was able to induce ENL depletion but faced challenges due to concurrent degradation of IKZF1, an undesirable off-target effect common to thalidomide-based PROTACs (*31*). IKZF1 is a crucial transcription factor in hematological cells, rendering its off-target degradation unfavorable. A similar scenario was observed with another thalidomide-based ENL PROTAC, Cpd-1, which, despite exhibiting antitumor activity, did not address the potential issue of off-target degradation of IKZF1 or other neo-substrates of CRBN:imides (*39*). Our approach, which focused on developing VHL-recruiting ENL PROTAC degraders, has overcome this limitation. This approach has led to MS41, which potently induces ENL degradation at low nanomolar concentrations. Our proteomic studies have revealed no detectable

off-target degradation of any proteins, including IKZF1, underscoring MS41's remarkable specificity. Because the parent ligand, PFI-6, is a dual inhibitor of ENL/AF9 YEATS domains, the derived MS41 does not distinguish between ENL and AF9. Nevertheless, since AF9 is not or lowly expressed in MV4;11 and many other *MLL*-r leukemia cells, the observed growth inhibitory effects primarily stem from ENL degradation. However, it remains crucial to continue efforts to develop PROTACs capable of selective degradation of ENL over AF9. In this regard, compound 7, an ENL-specific inhibitor recently developed by our team (*32*), emerges as a promising ENL binder for future development of ENL-specific PROTACs. In addition, TDI-11055, a recently reported small-molecule inhibitor of ENL (*34*), could also be used as an ENL binder for developing ENL PROTACs, owing to its in vivo efficacy in xenograft leukemia models.

In addition to *MLL*-r leukemia cell lines, our research has uncovered that KASUMI1, a leukemia cell line carrying the AML1-ETO translocation, is sensitive to MS41. This intriguing discovery suggests that MS41 may hold therapeutic potential beyond *MLL*-r leukemia (*58*). Furthermore, MS41 potently degrades YEATS domain mutant ENL and suppresses the aberrantly activated *HOXA* gene expression. This is exciting as these gain-of-function ENL YEATS mutations are prevalent in Wilms' tumor and have also been found in patients with AML (*53*–*55*). Together, these findings extend the therapeutic potential of MS41 to multiple cancers with diverse genetic backgrounds, underscoring the need for future clinical exploration.

MATERIALS AND METHODS

Chemistry general procedures

All chemical reagents were purchased from commercial vendors and used without further purification. The flash column chromatography was conducted using a Teledyne ISCO CombiFlash Rf + instrument. This instrument was also equipped with a variable-wavelength ultraviolet (UV) detector and a fraction collector. RediSep Rf Gold C18 columns were used for purification. High-performance liquid chromatography (HPLC) spectra for compounds were acquired using an Agilent 1200 series system with a diode-array detector (DAD). Chromatography was performed on a 2.1 mm Å ~ 150 mm Zorbax 300SB-C18 5-μm column with method (unless otherwise indicated) water containing 0.1% formic acid as solvent A and acetonitrile containing 0.1% formic acid as solvent B at a flow rate of 0.4 ml/min. The gradient program was as follows: 1% B (0 to 1 min), 1 to 99% B (1 to 4 min), and 99% B (4 to 8 min). Ultra-performance LC (UPLC) spectra for compounds were acquired using a Waters Acquity I-Class UPLC system with a photo diode array (PDA) detector. Chromatography was performed on a 2.1 mm Å ~ 30 mm Acquity UPLC BEH C18 1.7-μm column with water containing 3% acetonitrile, 0.1% formic acid as solvent A and acetonitrile containing 0.1% formic acid as solvent B at a flow rate of 0.8 ml/min. The gradient program was as follows: 1 to 99% B (1 to 1.5 min), and 99 to 1% B (1.5 to 2.5 min). High-resolution MS data were acquired in the positive ion mode using with Agilent G1969A API-TOF or with a Waters Acuity Premiere XE TOF with an electrospray ionization (ESI) source. Nuclear magnetic resonance (NMR) spectra were acquired on a Bruker DRX-400 spectrometer with 400 MHz for proton (^{1}H NMR) or 101 MHz for carbon (^{13}C NMR) or a Bruker DRX-600 spectrometer with 600 MHz for proton (^{1}H NMR). Chemical shifts are reported in parts per million (δ). Preparative HPLC was performed using an Agilent Prep 1200 series with UV detector set to 220 nm. Samples were injected into a Phenomenex Luna 75 mm Å ~ 30 mm, 5 μm, C18 column at room temperature (RT). The flow rate was 40 ml/min. A linear gradient was used with 10% of acetonitrile (A) in H_2O (with 0.1% trifluoroacetic acid) (B) to 100% of acetonitrile (A). All final compounds had >95% purity using the UPLC and HPLC methods described above. Synthesis and characterization of compounds **1** to **15** and MS41N as well as the key intermediate **18** are described in Supplementary Methods (see "Synthesis of key intermediate 18" and "Synthesis of ENL degraders"). ^{1}H NMR, ^{13}C NMR, and LCMS spectra for MS41 and MS41N are also provided (figs. S11 and S12). Linkers **19** to **33** (see "Synthesis of ENL degraders") were synthesized following our previously reported procedures (*59*). PFI-6 and compound **16** were synthesized according to published procedures (*36*).

Plasmids

Plasmids used to knock out ENL in MV4;11 cells were reported previously (*8*). turboGFP-Luciferase plasmid was a gift from M. Konopleva, UT MD Anderson Cancer Center. sgRNA sequences targeting the human *VHL* gene were designed on the basis of a CRISPR sgRNA database (GeneScript) and cloned into lentiCRISPR v2 vector (Addgene #52961) (*60*). Human YEATS domains: ENL (amino acids 1 to 145), AF9 (amino acids 1 to 145), full-length GAS41, and YEATS2 (amino acids 201 to 332) were cloned in pET19b expression vectors to express His-tagged YEATS domain proteins (*32*). All primers used in plasmid construction were listed in table S8.

Recombinant protein expression and purification

The His-tagged YEATS domains from AF9, ENL, GAS41, and YEATS2 were expressed in *Escherichia coli* strain Rosetta 2(DE3) pLysS in the presence of 0.1 mM isopropyl β-D-1-thiogalactopyranoside at 16°C (start induction when the optical density at 600 nm reaches 0.8) for 18 hours. Induced cells were collected and suspended in cold lysis buffer [20 mM tris-HCl (pH 7.5), 500 mM NaCl, 20 mM imidazole, 1 mM phenylmethylsulfonyl fluoride, and 1X proteinase inhibitors cocktail] with lysozyme solution (0.5 mg/ml). Cells were further lysed using an APV high-pressure homogenizer with pressure between 800 and 1000 PSI. Cell lysate was clarified by centrifugation at 22,000*g* at 4°C. Ni–nitrilotriacetic acid resins (Invitrogen, catalog no.12901-15) were used to purify His-tagged YEATS domain proteins following the manufacturer's instructions. Proteins were eluted with elution buffer [20 mM tris-HCl (pH 7.5), 500 mM NaCl, and 250 mM imidazole] and dialyzed in dialysis buffer [50 mM Hepes (pH 7.4), 100 mM NaCl, and 20% glycerol] to remove imidazole. Proteins were adjusted to 0.5 mg/ml, aliquoted, and stored at −80°C for AlphaScreen assay.

AlphaScreen assay and IC_{50} determination

AlphaScreen assay was set up as described before (*32*). The AlphaScreen assay was carried out in 384-well OptiPlates (PerkinElmer, catalog no. 6007290). Assays were performed in 30-μl reaction in Alpha reaction buffer [50 mM Hepes (pH 7.4), 100 mM NaCl for AF9 and ENL or 300 mM NaCl for GAS41 and YEATS2, 0.1% bovine serum albumin, and 0.05% CHAPS]. Protein, peptide, and compounds were mixed and incubated for 1 hour at RT before adding Alpha donor and acceptor beads (AlphaScreen Histidine Detection Kit, PerkinElmer, catalog no. 6760619). Alpha signals were detected on the SYNERGY-NEO2 multi-mode reader (BioTek) 2 hours later.

Protein concentrations of AF9, ENL, GAS41, and YEATS2 YEATS domains in the reactions were 30, 300, 100, and 100 nM, respectively, and peptide concentrations were 30 nM. For IC_{50} determination, compounds were subjected to 12 threefold serial dilutions for a total of 13 concentrations ranging from 54 μM to 0.1 nM to generate dose response curves. IC_{50} values were determined using nonlinear regression of variable slope (four parameters) curve fitting using GraphPad Prism.

Cell culture, virus transduction and drug treatment

Human leukemia cell lines MV4;11, RS4;11, KASUMI1, SEMK2, Jurkat, and K-562 were maintained in RPMI 1640 (Corning, catalog no. 10-040-CV) supplemented with 10% fetal bovine serum (FBS), 2 mM L-glutamine, and penicillin-streptomycin (100 U/ml; Corning, catalog no. 30-009-CI). HEK cell lines HEK293 and HEK293T were maintained in minimum essential medium (MEM, Corning, catalog no. 10-010-CV) and Dulbecco's modified Eagle's medium (DMEM, Corning, catalog no. 10-017-CV) with supplements, respectively. All human cell lines were mycoplasma-negative and were tested for authentication by short tandem repeat profiling performed by American Type Culture Collection or by UT MD Anderson Cancer Center CCSG core. Lentivirus packaging was performed in HEK293T cells, using X-treme GENE HP DNA transfection reagent (Roche, catalog no. 06366546001) in accordance with the manufacturer's instructions. The medium containing virus was centrifuged and concentrated using Amicon Ultra-15 columns. Spin infection was performed at 1,500 rcf at 25°C for 90 min, and transduced cell populations were usually selected or sorted 48 hours after infection.

For DC_{50} and D_{max} determination, leukemia cells were treated with increasing concentrations of MS41 ranging from 0.25 to 256 nM for 24 hours. Dose-dependent ENL degradation curves were generated on the basis of immunoblotting of ENL and β-Actin. DC_{50} values were determined using nonlinear regression of variable slope (four parameters) curve fitting using GraphPad Prism. In washout experiment, MV4;11 cells were first treated with 100 nM MS41 for 24 hours. MS41-containing medium was removed, and MV4;11 cells were washed with phosphate-buffered saline (PBS) twice. Then, the cells were cultured in normal medium and collected for Western blot analysis at the indicated time points.

Immunoblotting

Cells were lysed in cell lysis buffer [50 mM tris-HCl (pH7.4), 250 mM NaCl, 0.5% Triton X-100, and 10% glycerol] freshly supplemented with 1 mM dithiothreitol (DTT) and protease inhibitors. Protein concentration was measured by Bradford assay. Equal amounts of protein lysate were used for immunoblotting. Antibodies used in immunoblotting were list in table S9.

Proteomics sample preparation

DMSO and MS41-treated MV4;11 cells were collected at 2 and 6 hours after treatment. One million cells were collected for each sample. The cell pellets were resuspended in 8 M urea and 50 mM tris-HCl (pH 8.0), reduced with DTT (5 mM final) for 30 min at RT, and alkylated with iodoacetamide (15 mM final) for 45 min in the dark at RT. Samples were diluted fourfold with 25 mM tris-HCl (pH 8.0) and 1 mM $CaCl_2$ and digested with trypsin at a ratio of 1:100 (w/w, trypsin: protein) overnight at RT. There were three biological samples at each condition and total nine samples for one set. Peptides were cleaned by homemade C18 stage tips, and the concentration was determined (Peptide assay, Thermo Fisher Scientific, 23275). Twenty-five micrograms of each was used for labeling with isobaric stable tandem mass tags (TMT^{10}-126, 127N, 127C, 128N, 128C, 129N, 129C, 130N, 130C, Thermo Fisher Scientific, San Jose, CA) following the manufacturer's instruction. The mixture of labeled peptides was fractionated into 20 fractions on C18 stage tip with buffer 10 mM trimethylammonium bicarbonate (pH 8.5) containing 5 to 50% acetonitrile.

MS analysis

Dried peptides were dissolved in 0.1% formic acid and 2% acetonitrile. A total of 0.5 μg of peptides of each fraction was analyzed on a Q-Exactive HF-X coupled with an Easy nanoLC 1200 (Thermo Fisher Scientific, San Jose, CA). Peptides were loaded on to a nanoEase MZ HSS T3 column (100 Å, 1.8 μm, 75 μm by 250 mm, Waters). Analytical separation of all peptides was achieved with 110-min gradient. A linear gradient of 5 to 10% buffer B over 5 min, 10 to 31% buffer B over 70 min, and 31 to 75% buffer B over 15 min was executed at a 250 nl/min flow rate followed a ramp to 100%B in 1 min and 19-min wash with 100%B, where buffer A was aqueous 0.1% formic acid, and buffer B was 80% acetonitrile and 0.1% formic acid. MS experiments were also carried out in a data-dependent mode with full MS [externally calibrated to a resolution of 60,000 at mass/charge ratio (m/z) 200] followed by high-energy collision–activated dissociation–(tandem MS) MS/MS of the top 10 most intense ions with a resolution of 45,000 at m/z 200. High-energy collision–activated dissociation-MS/MS was used to dissociate peptides at a normalized collision energy of 32 eV in the presence of nitrogen bath gas atoms. Dynamic exclusion was 45 s.

Raw proteomics data processing and analysis

Peptide identification and quantification with TMT reporter ions were performed using the MaxQuant software version 2.1.0.0 (Max Planck Institute, Germany). Protein database searches were performed against the UniProt human protein sequence database (UP000005640). A FDR for both peptide-spectrum match and protein assignment was set at 1%. Search parameters included up to two missed cleavages at Lys/Arg on the sequence, oxidation of methionine, and protein N-terminal acetylation as a dynamic modification. Carbamidomethylation of cysteine residues was considered as a static modification. Peptide identifications are reported by filtering of reverse and contaminant entries and assigning to their leading razor protein. Data processing and statistical analysis were performed on Perseus (version 1.6.10.50). Protein quantitation was performed on biological replicates, and a two-sample t test statistics was used with a P value of 5% to report statistically significant protein abundance fold changes.

Cell viability assay

A total of 3500 cells were seeded in 96-well plate in 100 μl of medium, treated with DMSO or compounds at the indicated concentrations for 6 days. For cell lines less sensitive to MS41, a total of 1×10^5 cells were seeded in 12-well plate in 1 ml of medium, treated with DMSO or compounds at indicated concentrations for 12 days. The cells were passaged every 3 days with fresh compounds replenished. Cell viability was measured using the CellTiter-Glo luminescent cell viability assay kit (Promega, catalog no. G9241) according to the manufacturer's instructions. The surviving cells were calculated as percentage relative to the DMSO treated cells. Dose response curves were generated using GraphPad with nonlinear regression of variable

slope (four parameters) curve fitting, and IC_{50} values were determined from the plots.

Colony formation assay

Colony formation experiments were performed in Methocult (STEMCELL Technologies, catalog no. H4100). Eight thousand leukemia cells were resuspended in 400 μl RPMI 1640 medium and mixed with 4 ml complete Methocult medium. Triplicates of 1-ml cell suspension were added to six-well plates. Seven to ten days later, colonies were scanned and counted by Celigo (Nexcelom).

Cell cycle and apoptosis assay

Cells were harvested at the indicated time points. DAPI (4′,6-diamidino-2-phenylindole)–alcohol fixation method was used for cell cycle analysis. The cells were resuspended in 50 μl of Hanks' balanced salt solution (HBSS) containing 2% FBS, and then 1 ml of ice-cold 70% ethanol was added in a dropwise manner for fixation. Fixed cells were washed twice with HBSS containing 2% FBS and incubated with 1 ml of DAPI working solution (10 μg/ml DAPI and 0.1% Triton X-100 in PBS) in dark for 15 to 30 min at RT. The cells were filtered through 40-μm mesh filter and ready for flow cytometry analysis. Fluorescein isothiocyanate (FITC) annexin V Apoptosis Detection Kit (BD Pharmingen, catalog no. 556547) was used for cell apoptosis analysis. Cells were collected and washed twice with cold PBS and then resuspended in 1× binding buffer at a concentration of 1×10^6 cells/ml. One hundred microliters of resuspended cells were stained with 5 μl of FITC-annexin V and 2 μl of propidium iodide at RT for 15 min. Four hundred microliters of 1× binding buffer was added before flow cytometry analysis within 1 hour.

Drug synergy test

MV4;11 cells were treated with DMSO, MS41, doxorubicin (Sigma-Aldrich, catalog no. D1515), or combination of MS41 and doxorubicin at indicated concentrations for 6 days. Cell viability was measured using the CellTiter-Glo luminescent cell viability assay kit (Promega, catalog no. G9241) according to the manufacturer's instructions. Potential synergistic or antagonistic interaction was evaluated by Bliss independent response surface model (*61*).

RNA extraction and RT-qPCR analyses

Total RNA was isolated using the RNeasy Mini kit (Qiagen, catalog no. 74134) and reverse transcribed with the iScript cDNA Synthesis Kits (Bio-Rad, catalog no. 1708840) in accordance with the manufacturer's instructions. Quantitative real-time PCR was performed using the Power SYBR Green PCR Master Mix (Applied Biosystems, catalog no. A25742) with Bio-Rad CFX96 Real-Time system (C1000 Touch Thermal Cycler). The relative gene expression was calculated with the comparative C_T method by comparing the Ct value of a target gene to that of an internal control such as glyceraldehyde-3-phosphate dehydrogenase ($2^{\Delta\Delta CT}$). Primers used for RT-qPCR are provided in table S8.

RNA-seq and analysis

RNA was isolated as described above, and then sample libraries were prepared using the TruSeq RNA Sample Preparation Kit v2 (Illumina) in accordance with the manufacturer's instructions. RNA-seq samples were sequenced using Illumina NovaSeq 6000. Raw reads were mapped to human reference genome (hg38) by HISAT2 (v2.1.0) (*62*) with -k 1. CPM (counts per million) and fold change values were calculated by HTSeq (v0.11.3) (*63*) with --stranded = no -a 0 and edgeR (v3.16.5) (*64*) with trimmed mean of M-values and Exact test model. DEGs were filtered by FDR < 0.05 and FC > 1.5. Heatmaps were visualized by Java TreeView (v1.2.0). Gene Ontology biological processes term enrichment was done by DAVID 6.8 (*65*, *66*). GSEA (v4.3.2) (*50*) was used for GSEA with all curated gene sets v7.2 (gene sets can be downloaded at https://data.broadinstitute.org/gsea-msigdb/msigdb/release/7.2/c2.all.v7.2.symbols.gmt) and selected gene sets (*8*) with 1000 gene set permutations. Normalized RNA-seq data were rank-ordered by expression $\log_2$ fold change from edgeR. The normalized enrichment score (NES) provides the degree to which a gene set is overrepresented at the top or bottom of a ranked list of genes. The nominal *P* value describes the statistical significance of the enrichment score. The FDR *q* value is the estimated probability that a gene set with a given NES represents a false-positive finding. The selected gene sets used in this study are provided in table S4. Volcano plots for gene expression with $\log_2$ fold changes and $-\log_{10}$ FDR values, and *x*-*y* plots for GSEA curated gene sets results with NES and FDR values were generated by GraphPad Prism 10. ComBat-seq (*67*) was applied to remove batch effects in biological replicates of the $hCD45^+$ RNA-seq raw reads table, arising from flow cytometer sorting.

ChIP and ChIP-seq analysis

ChIP analysis was performed essentially as described previously with different sonication method (*19*, *68*). In brief, for ENL, H3K79me2, H3K4me3, H3K27ac, DOT1L, AFF4, RNA Pol II, and Pol II S2P ChIP experiments, cells were cross-linked with 1% formaldehyde for 10 min at RT and stopped with 125 mM glycine. For CDK9 ChIP, cells were cross-linked with 2 mM DSG cross-linker (Proteochem, catalog no. C1104) for 30 min at RT before cross-linking with 1% formaldehyde. Fixed cells were suspended in cell lysis buffer [5 mM PIPES (pH 8.0), 85 mM KCl, and 1% NP-40] to extract nuclei. For ENL and H3K79me2 ChIP, isolated nuclei were resuspended in nuclei lysis buffer [50 mM tris (pH 8.0), 10 mM EDTA, and 1% SDS] and sonicated using Covaris (E220 Evolution). For DOT1L, AFF4, CDK9, RNA Pol II, and Pol II S2P ChIP, isolated nuclei were resuspended in MNase digestion buffer [50 mM tris (pH 8.0), 1 mM $CaCl_2$, and 300 mM sucrose], and treated with 0.8 μl MNase (50 U/μl, Worthington, catalog no. LS004798) for 10 min at 37°C and stopped with 10 μl of 0.5 M EDTA. Samples were immunoprecipitated with 2 to 4 μg of antibodies overnight at 4°C. Thirty microliters of Protein A Dynabeads (Invitrogen, catalog no. 10002D) were then added and incubated at 4°C for 2 hours. The immunoprecipitates were washed twice with low-salt wash buffer [20 mM tris (pH 8.0), 150 mM NaCl, 2 mM EDTA, 1% Triton X-100, and 0.1% SDS], twice with high-salt wash buffer [20 mM tris (pH 8.0), 500 mM NaCl, 2 mM EDTA, 1% Triton X-100, and 0.1% SDS], once with LiCl buffer [20 mM tris (pH 8.0), 250 mM LiCl, 1 mM EDTA, 1% NP-40, and 1% Na-deoxycholate], and once with TE buffer [10 mM tris (pH 8.0) and 1 mM EDTA]. Bound DNA was eluted in ChIP elution buffer, reverse cross-linked, and purified using PCR purification kit (Qiagen, catalog no. 28106). ChIP DNA was analyzed by qPCR on the Bio-Rad CFX96 Real-Time system (C1000 Touch Thermal Cycler) using the Power SYBR Green PCR Master Mix (Applied Biosystems, REF A25742). Antibodies used in ChIP assays were list in table S9.

ChIP-seq sample libraries were prepared using KAPA Hyper Prep Kit (Roche) following the manufacturer's instructions. ChIP-seq samples were sequenced using Illumina NovaSeq 6000. Fastq reads

were mapped to hg38 human genome by HISAT2 (v2.1.0) (*62*) with --no-spliced-alignment -k 1 -X 1000. ENL peaks were called by MACS2 (v2.1.2) (*69*) with –broad against input. To get unions between peaks, bed files were processed through the pipeline cat | bedtools sort | bedtools merge. Bedtools intersect was used for defining ENL bound genes. Bigwig files, heatmaps, and average profiles were generated by Deeptools (v3.5.2) (*70*). Tracks were visualized by IGV (v2.7.2) (*71*). ENL bound genes were separated into high and low groups by ROSE (v1.3.2) (*72*) in the similar way as defining super enhancers and typical enhancers. Violin plots from both ChIP-seq and RNA-seq data were generated by R library Vioplot (v0.4.0).

Animal experiments

All animal experiments were approved by and performed in accordance with the guidelines of the Institutional Animal Care and Use Committee at the Van Andel Institute.

Mouse PK study

A standard in vivo PK study was conducted for MS41 sodium salt using six male Swiss albino mice with three mice per time point design. The mice were administered intraperitoneally with solution formulation of MS41 sodium salt at a 50 mg/kg dose. The formulation of 5% v/v NMP, 45% v/v propylene glycol, and 50% v/v PEG-400 was used in the study. Sixty microliters of blood samples were collected from three mice at each of the six time points (0.5, 1.5, 3, 6, 12, and 24 hours). Plasma was harvested by centrifugation of blood and stored at −70° ± 10°C until analysis. MS41 concentrations in plasma samples were quantified by fit-for-purpose LC-MS/MS method (LLOQ: 5.05 ng/ml).

In vivo efficacy studies in disseminated AML models

For in vivo treatment, MS41 compound was solved in DMSO at 200 mg/ml and diluted 1:20 with PEG300 (Selleckchem, catalog no. S6704) to the finial concentration of 10 mg/ml. Vehicle solution was prepared the same way but without the addition of MS41. Six- to eight-week-old NSG mice (NOD.Cg-*Prkdc*^{scid} *Il2rg*^{tm1Wjl}/SzJ) were used in xenograft experiments. NSG mice were treated with acidified water (pH 2.5 to 3) containing enrofloxacin antibiotics (0.17 mg/ml) 1 week before and 2 weeks after irradiation and leukemia cell transplantation. NSG recipient mice accepted sublethal dose of total body irradiation (2 Gy), followed by transplantation of 0.5 million MV4;11-Luciferase cells through tail vein injection. The success of leukemia engraftment was evaluated by BLI of mice 10 days after transplantation after intraperitoneal injection of D-Luciferin (Goldbio, catalog no. LUCK-1G) at 150 mg/kg dose. Imaging was performed on AMI HTX in vivo imaging system (Spectral Instruments Imaging). Mice were then grouped by bioluminescence signals and treated with vehicle or MS41 (once daily by injection, 50 mg/kg, i.p.). The animals were monitored daily, and body weights were measured every 3 days throughout the treatment period. To assess leukemia progression, BLI was performed weekly, and PB was collected for human CD45 staining and flow cytometry analysis. Bone marrow, spleen, and PB cells were collected at the experimental end point, and stained with human CD45 antibody for flow cytometry analysis. Kaplan-Meier survival curves were generated by GraphPad Prism software.

Toxicity test

Six to eight-week-old C57BL/6J mice were treated with vehicle or MS41 (50 mg/kg) through intraperitoneal injection once daily for 30 consecutive days. The mice were monitored daily, and body weights were measured every 3 days throughout the treatment. Complete blood count (CBC) was measured every 10 days by VetScan HM5. At day 30, bone marrow, spleen, and PB cells were collected and evaluated by flow cytometry. Cohorts of vehicle or MS41-treated mice were maintained for another 3 months after 30 days treatment. Body weight, CBC, and flow cytometry data from bone marrow, spleen, and PB were collected for evaluation of hematopoiesis after withdrawal of MS41 treatment.

Pathological evaluation of mouse tissue samples

Collected mouse tissues were fixed with 10% neutral buffered formalin (VWR, catalog no. 1600-128) for 48 hours. Bone marrow samples were decalcified through 45% sodium citrate / 20% formic acid (1:1 ratio) solution for 5 to 7 days. All tissues were processed, embedded, sectioned and stained in the Pathology and Biorepository Core at Van Andel Institute. Standard H&E and Ki-67 immunohistochemistry staining were performed with collected samples.

Flow cytometric analysis of hematopoietic and hematologic cells in bone marrow, PB, and spleen

Vehicle or MS41-treated C57BL/6J mice were euthanized, and bone marrow cells were isolated from femurs and tibia. Bone marrow cells were treated with 200 μl RBC lysis buffer (BioLegend, catalog no. 420301) for 2 min to remove RBCs. Collected PB cells were treated with 1 ml RBC lysis buffer for 15 min to remove RBCs. Sliced spleen was treated with 1-ml lysis buffer (HBSS +10 mg/ml collagenase D) for 15 min at 37°C, filtered with 75 μM mesh, and centrifuged at 500 rcf for 5 min at 4°C to collect splenocytes. Splenocytes were treated with 200 μl of RBC lysis buffer for 2 min to remove RBCs. Cells were stained with HSPC panel or Immune panel of antibodies (table S9) and analyzed on Aria Flow Cytometer (BD). Data were analyzed using Flow J software.

Fluorescence-activated cell sorting of hCD45$^+$ leukemia cells from mouse bone marrow

Bone marrow cells harvested from NSG mice xenografted with MV4;11 cells and treated with either vehicle or MS41 were stained with phycoerythrin anti-human CD45 (BioLegend, catalog no. 368510). The hCD45$^+$ cells, sorted using BD FACSymphony S6 cell sorter, were subsequently subjected to RNA extraction and RNA-seq analysis.

Statistical analyses

No statistical methods were used to predetermine the sample size. Experimental data are presented as means ± SEM unless stated otherwise. Statistical significance was calculated by a two-tailed, unpaired *t* test on two experimental conditions with $P < 0.05$ considered statistically significant unless stated otherwise. Statistical significance levels are denoted as follows: *$P < 0.05$; **$P < 0.01$; ***$P < 0.001$; and ****$P < 0.0001$.

Supplementary Materials

The PDF file includes:

Supplementary Methods
Figs. S1 to S12
Original blots for Fig. 5A
Legends for tables S1 to S9

Other Supplementary Material for this manuscript includes the following:

Tables S1 to S9

REFERENCES AND NOTES

1. A. C. Winters, K. M. Bernt, MLL-rearranged leukemias-an update on science and clinical approaches. *Front. Pediatr.* **5**, 4 (2017).
2. R. C. Rao, Y. Dou, Hijacked in cancer: The KMT2 (MLL) family of methyltransferases. *Nat. Rev. Cancer* **15**, 334–346 (2015).
3. R. Marschalek, MLL leukemia and future treatment strategies. *Arch. Pharm.* **348**, 221–228 (2015).
4. A. V. Krivtsov, S. A. Armstrong, MLL translocations, histone modifications and leukaemia stem-cell development. *Nat. Rev. Cancer* **7**, 823–833 (2007).
5. P. M. Ayton, M. L. Cleary, Molecular mechanisms of leukemogenesis mediated by MLL fusion proteins. *Oncogene* **20**, 5695–5707 (2001).
6. M. Mohan, C. Lin, E. Guest, A. Shilatifard, Licensed to elongate: A molecular mechanism for MLL-based leukaemogenesis. *Nat. Rev. Cancer* **10**, 721–728 (2010).
7. M. A. Erb, T. G. Scott, B. E. Li, H. Xie, J. Paulk, H. S. Seo, A. Souza, J. M. Roberts, S. Dastjerdi, D. L. Buckley, N. E. Sanjana, O. Shalem, B. Nabet, R. Zeid, N. K. Offei-Addo, S. Dhe-Paganon, F. Zhang, S. H. Orkin, G. E. Winter, J. E. Bradner, Transcription control by the ENL YEATS domain in acute leukaemia. *Nature* **543**, 270–274 (2017).
8. L. Wan, H. Wen, Y. Li, J. Lyu, Y. Xi, T. Hoshii, J. K. Joseph, X. Wang, Y. E. Loh, M. A. Erb, A. L. Souza, J. E. Bradner, L. Shen, W. Li, H. Li, C. D. Allis, S. A. Armstrong, X. Shi, ENL links histone acetylation to oncogenic gene expression in acute myeloid leukaemia. *Nature* **543**, 265–269 (2017).
9. D. Biswas, T. A. Milne, V. Basrur, J. Kim, K. S. Elenitoba-Johnson, C. D. Allis, R. G. Roeder, Function of leukemogenic mixed lineage leukemia 1 (MLL) fusion proteins through distinct partner protein complexes. *Proc. Natl. Acad. Sci. U.S.A.* **108**, 15751–15756 (2011).
10. N. H. He, M. Liu, J. Hsu, Y. H. Xue, S. Chou, A. Burlingame, N. J. Krogan, T. Alber, Q. Zhou, HIV-1 Tat and host AFF4 recruit two transcription elongation factors into a bifunctional complex for coordinated activation of HIV-1 transcription. *Mol. Cell* **38**, 428–438 (2010).
11. C. Lin, E. R. Smith, H. Takahashi, K. C. Lai, S. Martin-Brown, L. Florens, M. P. Washburn, J. W. Conaway, R. C. Conaway, A. Shilatifard, AFF4, a component of the ELL/P-TEFb elongation complex and a shared subunit of MLL chimeras, can link transcription elongation to leukemia. *Mol. Cell* **37**, 429–437 (2010).
12. D. Mueller, C. Bach, D. Zeisig, M. P. Garcia-Cuellar, S. Monroe, A. Sreekumar, R. Zhou, A. Nesvizhskii, A. Chinnaiyan, J. L. Hess, R. K. Slany, A role for the MLL fusion partner ENL in transcriptional elongation and chromatin modification. *Blood* **110**, 4445–4454 (2007).
13. A. Yokoyama, M. Lin, A. Naresh, I. Kitabayashi, M. L. Cleary, A higher-order complex containing AF4 and ENL family proteins with P-TEFb facilitates oncogenic and physiologic MLL-dependent transcription. *Cancer Cell* **17**, 198–212 (2010).
14. A. Shilatifard, R. C. Conaway, J. W. Conaway, The RNA polymerase II elongation complex. *Annu. Rev. Biochem.* **72**, 693–715 (2003).
15. E. Bitoun, P. L. Oliver, K. E. Davies, The mixed-lineage leukemia fusion partner AF4 stimulates RNA polymerase II transcriptional elongation and mediates coordinated chromatin remodeling. *Hum. Mol. Genet.* **16**, 92–106 (2007).
16. Y. Okada, Q. Feng, Y. Lin, Q. Jiang, Y. Li, V. M. Coffield, L. Su, G. Xu, Y. Zhang, hDOT1L links histone methylation to leukemogenesis. *Cell* **121**, 167–178 (2005).
17. K. M. Bernt, N. Zhu, A. U. Sinha, S. Vempati, J. Faber, A. V. Krivtsov, Z. Feng, N. Punt, A. Daigle, L. Bullinger, R. M. Pollock, V. M. Richon, A. L. Kung, S. A. Armstrong, MLL-rearranged leukemia is dependent on aberrant H3K79 methylation by DOT1L. *Cancer Cell* **20**, 66–78 (2011).
18. M. Mohan, H. M. Herz, Y. H. Takahashi, C. Lin, K. C. Lai, Y. Zhang, M. P. Washburn, L. Florens, A. Shilatifard, Linking H3K79 trimethylation to Wnt signaling through a novel Dot1-containing complex (DotCom). *Genes Dev.* **24**, 574–589 (2010).
19. Y. Li, H. Wen, Y. Xi, K. Tanaka, H. Wang, D. Peng, Y. Ren, Q. Jin, S. Y. Dent, W. Li, H. Li, X. Shi, AF9 YEATS domain links histone acetylation to DOT1L-mediated H3K79 methylation. *Cell* **159**, 558–571 (2014).
20. J. M. Schulze, A. Y. Wang, M. S. Kobor, YEATS domain proteins: A diverse family with many links to chromatin modification and transcription. *Biochem. Cell Biol.* **87**, 65–75 (2009).
21. J. M. Schulze, A. Y. Wang, M. S. Kobor, Reading chromatin: Insights from yeast into YEATS domain structure and function. *Epigenetics* **5**, 573–577 (2010).
22. Y. Li, B. R. Sabari, T. Panchenko, H. Wen, D. Zhao, H. Guan, L. Wan, H. Huang, Z. Tang, Y. Zhao, R. G. Roeder, X. Shi, C. D. Allis, H. Li, Molecular coupling of histone crotonylation and active transcription by AF9 YEATS domain. *Mol. Cell* **62**, 181–193 (2016).
23. A. J. Deshpande, J. Bradner, S. A. Armstrong, Chromatin modifications as therapeutic targets in MLL-rearranged leukemia. *Trends Immunol.* **33**, 563–570 (2012).
24. D. Mueller, M. P. Garcia-Cuellar, C. Bach, S. Buhl, E. Maethner, R. K. Slany, Misguided transcriptional elongation causes mixed lineage leukemia. *PLOS Biol.* **7**, e1000249 (2009).
25. A. Yokoyama, Leukemogenesis via aberrant self-renewal by the MLL/AEP-mediated transcriptional activation system. *Cancer Sci.* **112**, 3935–3944 (2021).
26. A. G. Muntean, J. L. Hess, The pathogenesis of mixed-lineage leukemia. *Annu. Rev. Pathol.* **7**, 283–301 (2012).
27. X. Li, X. M. Li, Y. Jiang, Z. Liu, Y. Cui, K. Y. Fung, S. H. E. van der Beelen, G. Tian, L. Wan, X. Shi, C. D. Allis, H. Li, Y. Li, X. D. Li, Structure-guided development of YEATS domain inhibitors by targeting π-π-π stacking. *Nat. Chem. Biol.* **14**, 1140–1149 (2018).
28. M. Moustakim, T. Christott, O. P. Monteiro, J. Bennett, C. Giroud, J. Ward, C. M. Rogers, P. Smith, I. Panagakou, L. Diaz-Saez, S. L. Felce, V. Gamble, C. Gileadi, N. Halidi, D. Heidenreich, A. Chaikuad, S. Knapp, K. V. M. Huber, G. Farnie, J. Heer, N. Manevski, G. Poda, R. Al-Awar, D. J. Dixon, P. E. Brennan, O. Fedorov, Discovery of an MLLT1/3 YEATS domain chemical probe. *Angew. Chem. Int. Ed. Engl.* **57**, 16302–16307 (2018).
29. T. Christott, J. Bennett, C. Coxon, O. Monteiro, C. Giroud, V. Beke, S. L. Felce, V. Gamble, C. Gileadi, G. Poda, R. Al-Awar, G. Farnie, O. Fedorov, Discovery of a selective inhibitor for the YEATS domains of ENL/AF9. *SLAS Discov.* **24**, 133–141 (2019).
30. J. N. Asiaban, N. Milosevich, E. Chen, T. R. Bishop, J. Wang, Y. Zhang, C. J. Ackerman, E. N. Hampton, T. S. Young, M. V. Hull, B. F. Cravatt, M. A. Erb, Cell-based ligand discovery for the ENL YEATS domain. *ACS Chem. Biol.* **15**, 895–903 (2020).
31. L. Garnar-Wortzel, T. R. Bishop, S. Kitamura, N. Milosevich, J. N. Asiaban, X. Zhang, Q. Zheng, E. Chen, A. R. Ramos, C. J. Ackerman, E. N. Hampton, A. K. Chatterjee, T. S. Young, M. V. Hull, K. B. Sharpless, B. F. Cravatt, D. W. Wolan, M. A. Erb, Chemical inhibition of ENL/AF9 YEATS domains in acute leukemia. *ACS Cent. Sci.* **7**, 815–830 (2021).
32. X. R. Ma, L. Xu, S. Xu, B. J. Klein, H. Wang, S. Das, K. Li, K. S. Yang, S. Sohail, A. Chapman, T. G. Kutateladze, X. Shi, W. R. Liu, H. Wen, Discovery of selective small-molecule inhibitors for the ENL YEATS domain. *J. Med. Chem.* **64**, 10997–11013 (2021).
33. X. Ni, A. T. Londregan, D. R. Owen, S. Knapp, A. Chaikuad, Structure and inhibitor binding characterization of oncogenic MLLT1 mutants. *ACS Chem. Biol.* **16**, 571–578 (2021).
34. Y. Liu, Q. Li, F. Alikarami, D. R. Barrett, L. Mahdavi, H. Li, S. Tang, T. A. Khan, M. Michino, C. Hill, L. Song, L. Yang, Y. Li, S. P. Pokharel, A. W. Stamford, N. Liverton, L. M. Renzetti, S. Taylor, G. F. Watt, T. Ladduwahetty, S. Kargman, P. T. Meinke, M. A. Foley, J. Shi, H. Li, M. Carroll, C. W. Chen, A. Gardini, I. Maillard, D. J. Huggins, K. M. Bernt, L. Wan, Small-molecule inhibition of the acyl-lysine reader ENL as a strategy against acute myeloid leukemia. *Cancer Discov.* **12**, 2684–2709 (2022).
35. X. Li, S. Liu, X. Li, X. D. Li, YEATS domains as novel epigenetic readers: Structures, functions, and inhibitor development. *ACS Chem. Biol.* **18**, 994–1013 (2023).
36. B. Raux, K. A. Buchan, J. Bennett, T. Christott, M. S. Dowling, G. Farnie, O. Fedorov, V. Gamble, C. Gileadi, C. Giroud, K. V. M. Huber, M. Korczynska, C. Limberakis, A. Narayanan, D. R. Owen, L. D. Saez, I. A. Stock, A. T. Londregan, Discovery of PFI-6, a small-molecule chemical probe for the YEATS domain of MLLT1 and MLLT3. *Bioorg. Med. Chem. Lett.* **98**, 129546 (2024).
37. H. Hu, A. G. Muntean, The YEATS domain epigenetic reader proteins ENL and AF9 and their therapeutic value in leukemia. *Exp. Hematol.* **124**, 15–21 (2023).
38. B. Dale, M. Cheng, K. S. Park, H. U. Kaniskan, Y. Xiong, J. Jin, Advancing targeted protein degradation for cancer therapy. *Nat. Rev. Cancer* **21**, 638–654 (2021).
39. X. Li, Y. Yao, F. Wu, Y. Song, A proteolysis-targeting chimera molecule selectively degrades ENL and inhibits malignant gene expression and tumor growth. *J. Hematol. Oncol.* **15**, 41 (2022).
40. J. Kronke, N. D. Udeshi, A. Narla, P. Grauman, S. N. Hurst, M. McConkey, T. Svinkina, D. Heckl, E. Comer, X. Li, C. Ciarlo, E. Hartman, N. Munshi, M. Schenone, S. L. Schreiber, S. A. Carr, B. L. Ebert, Lenalidomide causes selective degradation of IKZF1 and IKZF3 in multiple myeloma cells. *Science* **343**, 301–305 (2014).
41. G. Lu, R. E. Middleton, H. Sun, M. Naniong, C. J. Ott, C. S. Mitsiades, K. K. Wong, J. E. Bradner, W. G. Kaelin Jr., The myeloma drug lenalidomide promotes the cereblon-dependent destruction of Ikaros proteins. *Science* **343**, 305–309 (2014).
42. M. Ishoey, S. Chorn, N. Singh, M. G. Jaeger, M. Brand, J. Paulk, S. Bauer, M. A. Erb, K. Parapatics, A. C. Muller, K. L. Bennett, G. F. Ecker, J. E. Bradner, G. E. Winter, Translation termination factor GSPT1 is a phenotypically relevant off-target of heterobifunctional phthalimide degraders. *ACS Chem. Biol.* **13**, 553–560 (2018).
43. C. Galdeano, M. S. Gadd, P. Soares, S. Scaffidi, I. Van Molle, I. Birced, S. Hewitt, D. M. Dias, A. Ciulli, Structure-guided design and optimization of small molecules targeting the protein-protein interaction between the von Hippel-Lindau (VHL) E3 ubiquitin ligase and the hypoxia inducible factor (HIF) alpha subunit with in vitro nanomolar affinities. *J. Med. Chem.* **57**, 8657–8663 (2014).
44. K. Raina, J. Lu, Y. Qian, M. Altieri, D. Gordon, A. M. Rossi, J. Wang, X. Chen, H. Dong, K. Siu, J. D. Winkler, A. P. Crew, C. M. Crews, K. G. Coleman, PROTAC-induced BET protein degradation as a therapy for castration-resistant prostate cancer. *Proc. Natl. Acad. Sci. U.S.A.* **113**, 7124–7129 (2016).
45. S. Su, Z. Yang, H. Gao, H. Yang, S. Zhu, Z. An, J. Wang, Q. Li, S. Chandarlapaty, H. Deng, W. Wu, Y. Rao, Potent and preferential degradation of CDK6 via proteolysis targeting chimera degraders. *J. Med. Chem.* **62**, 7575–7582 (2019).
46. J. Wei, J. Hu, L. Wang, L. Xie, M. S. Jin, X. Chen, J. Liu, J. Jin, Discovery of a first-in-class mitogen-activated protein kinase kinase 1/2 degrader. *J. Med. Chem.* **62**, 10897–10911 (2019).
47. X. Yu, D. Li, J. Kottur, Y. Shen, H. S. Kim, K. S. Park, Y. H. Tsai, W. Gong, J. Wang, K. Suzuki, J. Parker, L. Herring, H. U. Kaniskan, L. Cai, R. Jain, J. Liu, A. K. Aggarwal, G. G. Wang, J. Jin, A selective WDR5 degrader inhibits acute myeloid leukemia in patient-derived mouse models. *Sci. Transl. Med.* **13**, eabj1578 (2021).

48. Y. Shen, G. Gao, X. Yu, H. Kim, L. Wang, L. Xie, M. Schwarz, X. Chen, E. Guccione, J. Liu, M. T. Bedford, J. Jin, Discovery of first-in-class protein arginine methyltransferase 5 (PRMT5) degraders. *J. Med. Chem.* **63**, 9977–9989 (2020).
49. J. Frost, C. Galdeano, P. Soares, M. S. Gadd, K. M. Grzes, L. Ellis, O. Epemolu, S. Shimamura, M. Bantscheff, P. Grandi, K. D. Read, D. A. Cantrell, S. Rocha, A. Ciulli, Potent and selective chemical probe of hypoxic signalling downstream of HIF-α hydroxylation via VHL inhibition. *Nat. Commun.* **7**, 13312 (2016).
50. A. Subramanian, P. Tamayo, V. K. Mootha, S. Mukherjee, B. L. Ebert, M. A. Gillette, A. Paulovich, S. L. Pomeroy, T. R. Golub, E. S. Lander, J. P. Mesirov, Gene set enrichment analysis: A knowledge-based approach for interpreting genome-wide expression profiles. *Proc. Natl. Acad. Sci. U.S.A.* **102**, 15545–15550 (2005).
51. T. C. P. Somervaille, M. L. Cleary, Identification and characterization of leukemia stem cells in murine MLL-AF9 acute myeloid leukemia. *Cancer Cell* **10**, 257–268 (2006).
52. A. Liberzon, C. Birger, H. Thorvaldsdottir, M. Ghandi, J. P. Mesirov, P. Tamayo, The Molecular Signatures Database hallmark gene set collection. *Cell Syst.* **1**, 417–425 (2015).
53. E. J. Perlman, S. Gadd, S. T. Arold, A. Radhakrishnan, D. S. Gerhard, L. Jennings, V. Huff, J. M. Guidry Auvil, T. M. Davidsen, J. S. Dome, D. Meerzaman, C. H. Hsu, C. Nguyen, J. Anderson, Y. Ma, A. J. Mungall, R. A. Moore, M. A. Marra, C. G. Mullighan, J. Ma, D. A. Wheeler, O. A. Hampton, J. M. Gastier-Foster, N. Ross, M. A. Smith, MLLT1 YEATS domain mutations in clinically distinctive Favourable Histology Wilms tumours. *Nat. Commun.* **6**, 10013 (2015).
54. S. Gadd, V. Huff, A. L. Walz, A. Ooms, A. E. Armstrong, D. S. Gerhard, M. A. Smith, J. M. G. Auvil, D. Meerzaman, Q. R. Chen, C. H. Hsu, C. Yan, C. Nguyen, Y. Hu, L. C. Hermida, T. Davidsen, P. Gesuwan, Y. Ma, Z. Zong, A. J. Mungall, R. A. Moore, M. A. Marra, J. S. Dome, C. G. Mullighan, J. Ma, D. A. Wheeler, O. A. Hampton, N. Ross, J. M. Gastier-Foster, S. T. Arold, E. J. Perlman, A Children's Oncology Group and TARGET initiative exploring the genetic landscape of Wilms tumor. *Nat. Genet.* **49**, 1487–1494 (2017).
55. K. Hetzner, M. P. Garcia-Cuellar, C. Buttner, R. K. Slany, The interaction of ENL with PAF1 mitigates polycomb silencing and facilitates murine leukemogenesis. *Blood* **131**, 662–673 (2018).
56. L. Wan, S. Chong, F. Xuan, A. Liang, X. Cui, L. Gates, T. S. Carroll, Y. Li, L. Feng, G. Chen, S. P. Wang, M. V. Ortiz, S. K. Daley, X. Wang, H. Xuan, A. Kentsis, T. W. Muir, R. G. Roeder, H. Li, W. Li, R. Tjian, H. Wen, C. D. Allis, Impaired cell fate through gain-of-function mutations in a chromatin reader. *Nature* **577**, 121–126 (2020).
57. H. Hu, N. Saha, Y. Yang, E. Ahmad, L. Lachowski, U. Shrestha, V. Premkumar, J. Ropa, L. Chen, B. Teahan, S. Grigsby, R. Marschalek, Z. Nikolovska-Coleska, A. G. Muntean, The ENL YEATS epigenetic reader domain critically links MLL-ENL to leukemic stem cell frequency in t(11;19) Leukemia. *Leukemia* **37**, 190–201 (2023).
58. Y. Chen, Y. Ying, W. Ma, H. Ma, L. Shi, X. Gao, M. Jia, M. Li, X. Song, W. Kong, W. Chen, X. Zheng, T. A. Muluh, X. Wang, M. Wang, X. S. Shu, Targeting the epigenetic reader ENL inhibits super-enhancer-driven oncogenic transcription and synergizes with BET inhibition to suppress tumor progression. *Cancer Res.* **84**, 1237–1251 (2024).
59. X. Yu, J. Xu, L. Xie, L. Wang, Y. Shen, K. M. Cahuzac, X. Chen, J. Liu, R. E. Parsons, J. Jin, Design, synthesis, and evaluation of potent, selective, and bioavailable AKT kinase degraders. *J. Med. Chem.* **64**, 18054–18081 (2021).
60. N. E. Sanjana, O. Shalem, F. Zhang, Improved vectors and genome-wide libraries for CRISPR screening. *Nat. Methods* **11**, 783–784 (2014).
61. R. Ramsdale, R. N. Jorissen, F. Z. Li, S. Al-Obaidi, T. Ward, K. E. Sheppard, P. E. Bukczynska, R. J. Young, S. E. Boyle, M. Shackleton, G. Bollag, G. V. Long, E. Tulchinsky, H. Rizos, R. B. Pearson, G. A. McArthur, A. S. Dhillon, P. T. Ferrao, The transcription cofactor c-JUN mediates phenotype switching and BRAF inhibitor resistance in melanoma. *Sci. Signal.* **8**, ra82 (2015).
62. D. Kim, J. M. Paggi, C. Park, C. Bennett, S. L. Salzberg, Graph-based genome alignment and genotyping with HISAT2 and HISAT-genotype. *Nat. Biotechnol.* **37**, 907–915 (2019).
63. S. Anders, P. T. Pyl, W. Huber, HTSeq—A Python framework to work with high-throughput sequencing data. *Bioinformatics* **31**, 166–169 (2015).
64. M. D. Robinson, D. J. McCarthy, G. K. Smyth, edgeR: A bioconductor package for differential expression analysis of digital gene expression data. *Bioinformatics* **26**, 139–140 (2010).
65. D. W. Huang, B. T. Sherman, R. A. Lempicki, Bioinformatics enrichment tools: Paths toward the comprehensive functional analysis of large gene lists. *Nucleic Acids Res.* **37**, 1–13 (2009).
66. D. W. Huang, B. T. Sherman, R. A. Lempicki, Systematic and integrative analysis of large gene lists using DAVID bioinformatics resources. *Nat. Protoc.* **4**, 44–57 (2009).
67. Y. Zhang, G. Parmigiani, W. E. Johnson, *ComBat-seq*: Batch effect adjustment for RNA-seq count data. *NAR Genom. Bioinform.* **2**, lqaa078 (2020).
68. L. Xu, H. Xuan, W. He, L. Zhang, M. Huang, K. Li, H. Wen, H. Xu, X. Shi, TAZ2 truncation confers overactivation of p300 and cellular vulnerability to HDAC inhibition. *Nat. Commun.* **14**, 5362 (2023).
69. Y. Zhang, T. Liu, C. A. Meyer, J. Eeckhoute, D. S. Johnson, B. E. Bernstein, C. Nusbaum, R. M. Myers, M. Brown, W. Li, X. S. Liu, Model-based analysis of ChIP-Seq (MACS). *Genome Biol.* **9**, R137 (2008).
70. F. Ramirez, D. P. Ryan, B. Gruning, V. Bhardwaj, F. Kilpert, A. S. Richter, S. Heyne, F. Dundar, T. Manke, deepTools2: A next generation web server for deep-sequencing data analysis. *Nucleic Acids Res.* **44**, W160–W165 (2016).
71. J. T. Robinson, H. Thorvaldsdottir, W. Winckler, M. Guttman, E. S. Lander, G. Getz, J. P. Mesirov, Integrative genomics viewer. *Nat. Biotechnol.* **29**, 24–26 (2011).
72. W. A. Whyte, D. A. Orlando, D. Hnisz, B. J. Abraham, C. Y. Lin, M. H. Kagey, P. B. Rahl, T. I. Lee, R. A. Young, Master transcription factors and mediator establish super-enhancers at key cell identity genes. *Cell* **153**, 307–319 (2013).

Acknowledgments: We thank members of the Wen and Jin laboratories for technical support and scientific discussion throughout the study. We also thank C. Krawczyk and L. Zhai at Van Andel Institute for helping with flow cytometry panels to evaluate mouse hematopoiesis. We gratefully acknowledge the support and services provided by the Core Technologies and Service at Van Andel Institute (VAI), including M. Adams and the Genomics Core (RRID:SCR_022913) for NGS sequencing, R. Sheridan and the Flow Cytometry Core (RRID:SCR_022685) for assistance with flow cytometry data collection and analysis, the Vivarium (RRID:SCR_023211) for maintenance of mouse colonies, the Pathology and Biorepository Core (RRID:SCR_022912) for assistance with tissue sample staining, and Z. Madaj and the Bioinformatics and Biostatistics Core for assistance with power calculation. Computation for the work described here was supported by the High-Performance Cluster and Cloud Computing (HPC3) resource at the VAI. **Funding:** This work was supported in part by grants from the National Institutes of Health (NIH) (R01CA260666 to J.J. and H.W.; R01CA255506 to H.W.; R21AG071229, R41DK133051-01A1, and R01GM133107-01 to X.C.; and R01CA268440 to X.S.) and the Leukemia & Lymphoma Society (LLS) (Career Development Program Scholar award 1387-23 to H.W.). This work used the NMR Spectrometer Systems at Mount Sinai acquired with funding from NIH's Shared Instrument grants 1S10OD025132 and 1S10OD028504. **Author contributions:** Conceptualization: H.W. and J.J. Methodology: H.W., J.J., Z.X., L.Q., H.Ü.K., X.C., and X.S. Data curation: Z.X., L.Q., H.X., K.L., M.H., L.X., Y.S., L.X.X., J.H., and B.D. Investigation: Z.X., L.Q., H.X., L.X., and H.Ü.K. Visualization: H.W., Z.X., H.X., and H.Ü.K. Supervision: H.W. and J.J. Writing—original draft: H.W., J.J., Z.X., H.X., and H.Ü.K. Writing—review and editing: H.W., Z.X., H.X., J.J., H.Ü.K., and X.S. **Competing interests:** A patent application filed by Icahn School of Medicine at Mount Sinai and Van Andel Institute for ENL PROTACs is pending. J.J. is a cofounder and equity shareholder in Cullgen Inc.; a scientific cofounder and scientific advisory board member of Onsero Therapeutics Inc.; and a consultant for Cullgen Inc., EpiCypher Inc., Accent Therapeutics Inc., and Tavotek Biotherapeutics Inc. The Jin laboratory received or has received research funds from Celgene Corporation, Levo Therapeutics Inc., Cullgen Inc., and Cullinan Oncology Inc. The authors declare that they have no other competing interests. **Data and materials availability:** The ChIP-seq and RNA-seq data have been deposited in the Gene Expression Omnibus database under accession numbers GSE245927. All data needed to evaluate the conclusions in the paper are present in the paper and/or the Supplementary Materials.

Submitted 19 January 2024
Accepted 24 July 2024
Published 28 August 2024
10.1126/sciadv.ado1432